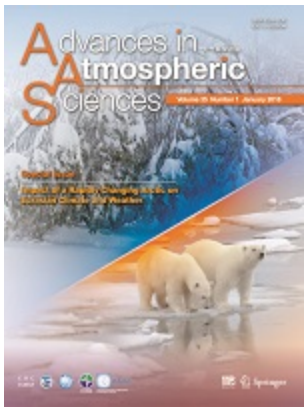

Evidence of Specific MJO Phase Occurrence with Summertime California Central Valley Extreme Hot Weather

Journal:	*Advances in Atmospheric Sciences*
Manuscript ID	AAS-2018-0167.R1
Manuscript Type:	Original Article
Date Submitted by the Author:	n/a
Complete List of Authors:	Lee, Yun-Young; APEC Climate Centre Grotjahn, Richard; University of California, L.A.W.R.

SCHOLARONE™
Manuscripts

Evidence of Specific MJO Phase Occurrence with Summertime California Central Valley Extreme Hot Weather

Yun-Young Lee[1] and Richard Grotjahn[2]

[1]*APEC Climate Center, Busan, South Korea*

[2]*Department of Land, Air and Water Resources, University of California, USA*

For Review Only

August 2018

To be submitted to Advances in Atmospheric Science

* *Corresponding author address*:

Richard Grotjahn, UC Davis, One Shields Ave. Davis, CA, 95616, U.S.A.

Email: grotjahn@ucdavis.edu

ABSTRACT

This study examines associations between California Central Valley (CCV) heat waves (HWs) and the Madden Julian Oscillation (MJO). This report is motivated by the fact that CCV HWs are frequently preceded by convection over the tropical Indian and eastern tropical Pacific Oceans, regions identifiable with MJO phases. The main analysis method examines lagged composites (formed after each MJO phase pair) of CCV synoptic stations temperature, Outgoing Longwave Radiation (OLR), and Velocity Potential (VP). Over the CCV, positive temperature anomalies are observed only after the Indian Ocean (phases 2-3) or eastern Pacific Ocean (phases 8-1) convection (implied by OLR and VP fields). The largest fractions of the CCV hot days occur during those two phase pairs. OLR and VP composites have significant subsidence and convergence above divergence over the CCV during HWs and these structures are part of a larger pattern extending into the subtropical eastern Pacific during MJO phase pairs 2-3 and 8-1.

Prior studies showed that CCV HWs are roughly grouped into two clusters: Cluster 2 is preceded by a HW over northwest North America while Cluster 1 is not. OLR and VP composite analyses are applied separately to these two clusters. However, for Cluster 2, the subsidence and VP over the CCV are not significant and the large scale VP pattern has small correlation to the MJO lagged composite field. Therefore, the association between MJO convection and subsequent CCV HW is more evident in Cluster 1 than Cluster 2.

For Review Only

Key words: Madden Julian Oscillation, California Central Valley heat waves, Madden Julian Oscillation links to California heat waves, Large Scale Meteorological Patterns, Extratropical response to tropical convection

Plain Language Summary: This study reveals connections between California extreme heat waves and enhanced convection (heavy precipitation) in specific regions of the tropics. That tropical convection is signified by pairs of phases in the Madden-Julian Oscillation, or MJO. The phases are identified using a standard index. Many summertime California heat waves (HWs) are preceded by MJO convection over 1) the Indian Ocean and Southeast Asia and 2) eastern tropical Pacific from 4 to 16 days earlier. There are two categories of California HWs, In one category the HW forms rapidly over California and is linked to unusually hot temperatures just off the northwest California coast; this type of heat wave is more strongly linked to the two areas of tropical convection than is the other category of HWs. The other type of HW is weakly linked to MJO convection only in the eastern tropical Pacific.

Three main points of the article:

1. Summertime California heat waves (HWs) are preceded by MJO convection in the Indian Ocean and Southeast Asia and eastern tropical Pacific.

2. In MJO phases 2-3 and 8-1, VP and OLR fields over California are part of a larger response extending into the subtropical eastern Pacific.

3. Cluster1 HWs (that form at California) are more linked to MJO phases than are Cluster 2 (from existing HWs that expand over California).

For Review Only

1. Introduction

The California Central Valley (CCV) summer is characterized by occasional events having very high temperature. Extreme hot days, here called heat waves (HWs), are not unusual in this area. These HWs have temperatures higher than 38 ^{o}C (100 ^{o}F) for three or more days in a row. The CCV produces half of the nation's tree fruit and nut crops and includes extensive dairy production. Extremely high temperatures degrade the quality and quantity of agricultural production and in severe events cause extensive cow fatalities. The frequency and intensity of summer temperature extremes have large impacts on the regional economy of the CCV. For example, the CCV dairy industry had ~1$B of economic losses from the 2006 HWs. Therefore, understanding the mechanisms that lead to CCV hot weather is very important.

During boreal winter season, extreme events have been linked to a blocking pattern and several climate modes such as: the Pacific-North American (PNA) pattern and North Atlantic Oscillation (NAO) (Brown et al. 2008; Cellitti et al. 2006; Downton and Miller 1993; Guirguis et al. 2011; Kenyon and Hegerl 2008; Lee and Black 2013; Loikith and Broccoli 2013; Sillmann et al. 2011; Walsh et al. 2001; Wettstein and Mearns 2002). There are substantial modulations of temperature extremes by the El Niño/Southern Oscillation (ENSO) (Alexander et al. 2009; Higgins et al. 2002; Lim and Schubert 2011; Meehl and Teng 2007). It has also been shown that temperature extremes are accompanied by large displacements of air masses that create specific wave patterns, so-called, large scale

For Review Only

meteorological patterns (LSMPs) reviewed in Grotjahn et al. (2016) that are distinct from climate modes mentioned above. Regional scale extreme heat in the CCV is shown to be linked to LSMPs that are an equivalent barotropic, nearly-stationary wave train (ridge-trough-ridge) across the North Pacific and western North America (Grotjahn 2011, 2013, 2016; Grotjahn and Faure 2008; Palipane and Grotjahn, 2018). Looking at the general features of LSMPs prior to HWs onset is a good way to connect those HWs with associated atmospheric phenomena and therefore begin to understand related mechanisms.

The Madden–Julian oscillation (MJO) is the dominant mode of intraseasonal variability in the tropics (Madden and Julian 1994; Madden and Julian 1972; Zhang 2005). However, its impacts are not limited to tropical latitudes and it has influences on the subtropical and extratropical flows in both hemispheres (Higgins and Mo 1997; Kiladis and Weickmann 1992; Lau and Phillips 1986; Matthews et al. 2004). Tropical convection associated with the MJO generally propagates eastward through the Indian and Pacific Ocean basins with the periodicity of 40–50 days (Madden and Julian 1994; Madden and Julian 1972). Wheeler and Hendon (2004) developed a seasonally independent index to monitor the MJO. Based on their definitions, a phase number indicates longitudes of enhanced convection in the MJO life cycle: during phases 2-3 convection is enhanced over the Indian Ocean, in phases 4-5 over the 'Maritime Continent', in phases 6-7 over the western Pacific, and in phases 8-1 over the Western Hemisphere as shown in OLR composites (Fig. 1). Purple boxes represent the active convective regions of the four phase pair categories. Phase pair 8-1 is called the eastern Pacific MJO phase in this study. Although MJO phase separation is less clear in summer than in winter (Wheeler and

For Review Only

Hendon 2004), the above classification is relevant enough to be applicable to summer MJO phases.

Enhanced sinking motion over western North America and just west-northwest of the CCV area is closely related with the onset of extreme CCV HWs (Lee and Grotjahn, 2016; hereafter LG2016). The sinking is strongest offshore but significant over the continent (Grotjahn, 2011). OLR composites in Fig.1 show high values (implying clear skies from descent) over western North America and offshore during active MJO convection of phase pair 2-3 but much less sinking motion during other phases. Therefore, the authors expect CCV area temperature extremes to be more likely after strong phase pair 2-3 of the MJO than after other phases. These results motivated this research into the MJO phase dependency of CCV hot weather.

Several researchers have shown MJO contributions to regional weather over diverse regions. The MJO strength and phase have influenced winter precipitation over East Asia (Jeong et al. 2008) and in North America and Canada (Lin et al. 2010; Zhou et al. 2012), and summer precipitation in Australia (Wheeler et al. 2009). The MJO phases also influence winter surface temperatures over East Asia (Jeong et al. 2005) and in North America (Lin and Brunet 2009; Schreck et al. 2013; Zhou et al. 2012). Schreck et al (2013) reveal that strong MJO contributes to *eastern* North America temperatures notably only when a specific PNA-like structure is present. Moon et al. (2011) show that MJO influence on temperature of the Canada and northwest US coasts is dependent on ENSO phase. Specifically, during MJO phase 3, those areas experience cold weather during La Niña while warm weather during El Niño. Under MJO phase 7, those areas experience warm and humid weather during El Niño.

For Review Only

MJO may influence the occurrence of extreme weather. Hong and Li (2009) show that the extreme cold anomaly over Southeast Asia in February 2008 occurred in association with Maritime Continent MJO phase accompanying a mature phase La Nina. Jones et al. (2010) demonstrate that forecast skill of extreme precipitation over the contiguous United States becomes higher with active and enhanced MJO convection during phases 1 and 8. Matsueda and Takaya (2015) demonstrate the global influence of the MJO on the extreme warm and cold conditions. However, most prior studies dealing with MJO influence on weather extreme emphasize the winter season. MJO association with summer season weather extremes has not been well explored yet to our knowledge. This study examines summer season hot weather in the CCV in association with MJO phases. Section 2 outlines the dataset and methods used. Section 3 examines which large scale pattern of tropical convection in specific MJO phases is preferable for occurrence of CCV hot weather. Section 4 presents differences in the MJO to CCV HWs association sorted by the two types of CCV HWs. Lastly, section 5 summarizes the results.

2. Data and Methodologies

This study considers boreal summer season extending from June through September (JJAS, 122 days) and the time period from 1979 to 2010 (32 years). During this period, 24 CCV summer HW events are isolated from the daily maximum near surface temperature time series at 15 NCDC (National Climatic Data Center) stations covering the whole CCV area. The criteria for identifying HWs are detailed in LG2016. Briefly, the criteria are that a majority of the CCV stations must have maximum temperature within the top 5% for each station simultaneously for at least three consecutive days. Two

For Review Only

temperature extreme metrics are defined to measure the HW severity. One metric is the average of normalized temperature anomalies within specified days after MJO phase pairs. Even within the CCV, how extreme one degree of temperature anomaly is varies a lot among stations. Therefore, temperature anomalies are first normalized by long-term daily mean standard deviation for each station to make all station values intercomparable. The other metric is the number of days (NODs) within the total number of 5% hottest days, that also occurs in each specified period after each MJO event; these NODs are then divided by the total number of days to define the occurrence fractions (chance) of hot days.

The MJO phase is based on the Real-time Multivariate MJO (RMM) index (Wheeler and Hendon 2004) obtained from the Australian Bureau of Meteorology data server (http://www3.bom.gov.au/twpice/forecast_trial/mjo/20050201/RMM1RMM2.74toRealtime.txt.1107263700). Only active MJO days are considered here and defined as those days when the RMM index has amplitude greater than or equal to one. This study simplifies the interpretation of the MJO relationships to CCV hot weather by emphasizing four zonal locations of tropical convection: Indian Ocean, Maritime Continent, western-central Pacific, and eastern Pacific. This emphasis is accomplished, by pairing two consecutive MJO phases (2-3, 4-5, 6-7, and 8-1) in all analyses here. To isolate sufficiently strong and discrete signals, MJO events are identified using three criteria when: i) the RMM index phase persists for at least 3 days with amplitude of one or larger, ii) the interval between two events is 10 days or longer, and iii) both start and end dates of events are within the summer season from June through September. This process isolates 57, 64, 52, and 59 events for MJO phase pairs 2-3, 4-5, 6-7, and 8-1, respectively. MJO events composites

For Review Only

clearly display the typical zonal locations of active convection during individual MJO phase pairs (Fig. 1).

The characteristics of MJO phase-dependent convective motion are analyzed using daily mean outgoing longwave radiation (OLR) in 1 degree latitude by 1 degree longitude grid intervals. The OLR data are from High Resolution Infrared Radiation Sounder (HIRS) radiance observations onboard the National Oceanic and Atmospheric Administration (NOAA) Television and Infrared Observation Satellite N (TIROS-N) series and European Organization for the Exploitation of Meteorological Satellites (Eumetsat) MetOp polar orbiting satellites (Lee et al. 2007). The data is available online at https://climatedataguide.ucar.edu/climate-data/outgoing-longwave-radiation-olr-hirs.

The upper and lower tropospheric divergence/convergence conditions associated with MJO convection are examined by analyzing the velocity potential (VP) derived from ERA-Interim data produced by the European Centre for Medium-Range Weather Forecasts (ECMWF) described by Dee et al. (2011). These data have 6 hourly temporal resolution and 1 degree longitude by 1 degree latitude spatial resolution and were obtained from http://apps.ecmwf.int/datasets/data/interim-full-daily/.

This study emphasizes anomaly, composite fields of OLR and VP from selected lag days after the MJO event onset date to understand MJO-related atmospheric conditions in the CCV environs. Those results are compared with composite fields made during CCV HW events. For the quantitative comparison, the pattern correlation analysis is applied over a large horizontal domain covering the Indian Ocean and Pacific Ocean from the tropics to extratropics (60°E-90°W, 10°S-50°N) in order to capture locations important in different MJO phases. Prior work (LG2016) found two different evolutions of the large scale wind,

For Review Only

mass, and temperature fields prior to CCV HW onset. Since the working hypothesis is that MJO phases preceding CCV HW onset may impact CCV HW properties, then composite and pattern correlation analyses are sorted on the basis of these two distinct HW types or clusters.

3. MJO phase dependency of CCV extreme hot weather occurrence

3.1 Tropical convection leading up to CCV hot weather

Some properties of the weather and climate in the extratropics seems to lag properties of the MJO (Jin and Hoskins 1995; Lin and Brunet 2009; Lin et al. 2009; Lin et al. 2010; Mori and Watanabe 2008; Schreck et al. 2013). Looking at OLR over a wide swath of the tropics and subtropics before CCV HW events onset gives hints at possible links between the tropics and the CCV.

Negative areas of OLR imply anomalously cold temperatures and in the tropics the low temperatures are interpreted as arising from higher cloud tops associated with stronger moist convection. Hence, enhanced convection and negative OLR will be used interchangeably in this article for convenience. Similarly, positive OLR anomalies are associated with lower cloud tops or less cloudiness than average. Hence positive OLR and enhanced subsidence will be used interchangeably. Figure 2a shows the OLR anomalies composite for 13 days prior to 24 CCV HW events. In daily composites, the Indian Ocean and tropical eastern Pacific have anomalously strong convective anomalies out to 13 days before days of hotter CCV temperatures (not shown). In Fig. 2a, tropical Indian Ocean has strong convection and it seems most closely related with phases 2-3 of MJO activity. While, western-central Pacific (MJO phases 6-7) has notable subsidence. Central America and

For Review Only

Mexico have relatively weak but significant convection to the south of 10°N (related to MJO phase pair 8-1).

The association between phase 2-3 MJO events and CCV extreme hot days is reinforced by another metric, shown in Fig. 2b. This metric first counts the number days assigned to each of the 4 MJO phase pairs when either member of the pair has large amplitude (RMM≥1) during the 13 days leading up to extreme CCV HW event onsets. Then, it is divided by the total number of days for 24 events (13 x 24 days) and the resultant active MJO days fraction is plotted as dark bars. Active phase pair 8-1 days occupy nearly 30% of the total number of days leading up to HWs, while active phase 4-5 days occupy less than 5%. Since the number of days each phase is 'active' varies, the fraction of all the summer days is also plotted (white bars). During 32 summer seasons, the fraction of active MJO phase days is rather similar and around 15% for each phase pair. Clearly, the fraction of days leading up to HWs for phase pair 8-1 is almost double the fraction of all summer days and this indicates that the eastern Pacific convection is strongly associated with CCV hot weather. The fraction of days in phase pair 2-3 is also slightly increased before HW onset. The other phases are less likely to occur before CCV HWs than to a summer day on average.

Significant OLR convection and frequent MJO fraction shown in Fig. 2 may imply that in terms of CCV HWs, a link to tropical convection is relevant and the association may vary with the geographical location of MJO convections. As a next step, this study examines CCV station temperature variation after each of the four different phase pairs in order to estimate when temperature changes appear related to a preceding MJO phase. In Fig. 3a, the 15 CCV stations' averaged normalized temperature anomalies (T_norm) are plotted at

For Review Only

individual lag days after each indicated MJO phase pair onset. For phase pair 8-1, CCV temperature peaks at lag day 12 but decreases gradually until dropping below zero after lag day 16. Phase pair 2-3 time series have relatively sharp peak at lag day 15 with slightly less T_norm compared to phase pair 8-1. For phase pair 4-5, CCV temperature anomaly stays under zero over all lag days. For phase pair 6-7, temperature starts negative crossing over zero after 15 days lag.

Figure 3b compares counts of extreme hot days averaged over the 15 CCV stations at different lags for the four MJO phase pairs. Extreme hot days are identified when the T_norm on the date are among the 5% hottest dates from all summer season days. The fraction of hot days is the largest during 7 to 14 days after the onset of the phase pair 8-1. It is relatively high during 14 to 16 for the phase pair 2-3. Generally, phase pair 4-5 and 6-7 has comparatively small fraction through all lag days. Longer lag for phase pair 2-3 than for phase pair 8-1 could be expected since the convection location of phase 8-1 is much closer to the CCV than is the location of phase 2-3 convection. This shorter distance argument is based in part on the assumption that some 'signal' from the convection could propagate at a roughly similar rate in the different directions needed to reach the CCV. However, this shorter distance argument breaks down when considering phase pair 6-7 has its highest fractions after phase pair 2-3 does. Also, the highest fraction for phase pair 2-3 is at zero lag. Based on the results of Fig. 3a and 3b, a time frame of 4 to 16 lag days after MJO events is selected as a consistent time frame over which the MJO phases are associated with CCV HWs.

Normalized temperature anomalies and hot days fractions are averaged over 4 to 16 days after MJO events onset and displayed in Figs. 3c and 3d. Temperature anomalies are

For Review Only

positive for phase pairs 2-3 and 8-1 while they are negative for phase pairs 4-5 and 6-7. The fraction of hot days for phase pair 8-1 is much larger than the other three phase pairs. Both temperature metrics have largest value in phase pair 8-1 and second largest value in phase pair 2-3. Thus, it is hypothesized that phase pair 8-1 MJO (eastern Pacific convection) and phase pair 2-3 MJO (Indian Ocean convection) have higher association with subsequent CCV extreme hot days with larger frequency and strong amplitude.

3.2 MJO-related LSMPs favorable for CCV hot weather: OLR and velocity potential

This section examines the CCV hot weather link to MJO phase by focusing on the broader extratropical large scale circulation patterns of OLR and VP following each phase pair of strong MJO events. The composites of each MJO phase pair for 4-16 days after active MJO events onset are compared to composites during HW events. Similarities in corresponding patterns between figures and the LSMPs in this section connect MJO occurrence and CCV weather.

Figure 4(a-d) displays the OLR anomaly composite of 4 to 16 days after MJO events onsets for four phase pairs. Due to the lag in time, OLR patterns are displaced not only eastward but also northward compared to the active days MJO composites centered on purple boxes (Fig. 1). Both negative and positive OLR (convection and subsidence) over the Indian Ocean to western Pacific region have a northwest to southeast elongation. The shift and shape of the OLR signal makes sense because northward propagation around Southeast Asia is a primary feature of the summertime MJO (Kiladis et al. 2014; Wang et al. 2018). After MJO phase pair 8-1, the main convective signal still remains inside the purple box (the tropical eastern Pacific). Outside the tropics, there are significant large positive

For Review Only

OLR values over the much of the western US only after the 2-3 and 8-1 phase pairs. Negative OLR is significant over western North America after the 4-5 and 6-7 phase pairs. The average OLR anomaly over an area is a proxy measure of local rising or sinking of air parcels. The green box area average of OLR (Fig. 4e) clearly shows that subsidence (ascending motion) of air in the CCV can be enhanced during MJO convection over the Indian or eastern Pacific Oceans (Maritime Continent or western Pacific). Robustness of the CCV subsidence signal is also estimated by the 'sign-fraction'; that measures anomaly sign consistency between composite members by counting the number of events with positive value of the anomaly and subtracting the number of events with negative value at that point then dividing it by the total number of events at each grid point, a procedure similar to normalized 'sign-counts' used by Lee and Grotjahn (2016). A sign fraction of -1.0 indicates all events have negative anomaly at that grid point while +1/3 indicates two thirds of all events have positive OLR anomaly. The subsidence over the CCV after both the 2-3 and 8-1 phase pairs is consistent by exceeding the 1/3 sign-fraction level (Fig. S1 in the supplementary information). However, enhanced negative OLR anomaly over the CCV after the 4-5 and 6-7 phase pairs is not consistent at that sign fraction level.

Central America and tropical eastern Pacific convective anomalies combined with strong subsidence anomalies over western North America are worth additional discussion. This pattern looks partly consistent with the vertical velocity pattern shown by Hoskins et al. (1999) in their Fig. 3; their figure shows the pattern on day 12 from a primitive equation model simulation being forced by heating over the so-called American monsoon region (0-60°N, 110°W-40°W). It was speculated that American Monsoon convection amplifies subtropical North Pacific sea level pressure anticyclones through enhanced descent

For Review Only

balanced by enhanced northerly winds on the eastern flank of those anticyclones (Hoskins 1996; Hoskins et al. 1999). However, later work (Grotjahn and Osman 2007) found observational evidence that the stronger Central American precipitation occurs *after* the stronger subtropical high. Furthermore, there is a theoretical basis for enhanced eastern Pacific and Central American convection to lead to subsidence to the north-northwest found in the Matsuno-Gill models (Gill 1980; Matsuno 1966). Although our study emphasizes extremes not the summer time mean state, a Rossby wave Matsuno-Gill response is also applicable to CCV temperature extremes after specific phase MJO convection.

The 8-1 MJO phase pair is followed by significant above-normal convection over the equatorial eastern Pacific and Central America northward to 25°N (Fig. 4d). Further north, over western America (green box), the OLR is significant and positive; prior works (Gershunov et al. 2009; Grotjahn 2011) find an anticyclone centered over the US Great Basin and Rocky Mountains. An anticyclone in this region can be generated by the Matsuno-Gill model. This enhanced inland anticyclone sets up a sea level pressure gradient to oppose a sea breeze that would otherwise cool the CCV (Grotjahn, 2011). Affiliated with that anticyclone produced by the Matsuno-Gill model and linked to western America hot weather, corresponding OLR maxima are seen in the composite for MJO phase pair 8-1.

The Laplacian of velocity potential measures the strength of divergence and convergence at a specific atmospheric level. Being related to divergence via the Laplacian, the VP field is much smoother spatially than the divergence field and that is why it is used here to identify very large scale structures associated with CCV HWs and MJO phases. A positive relative maximum in VP broadly indicats convergence, negative VP minimum

For Review Only

implies divergence. Therefore VP fields also imply vertical motion. Between convergence aloft and divergence below, air parcels sink and their sensible temperature increases adiabatically. It is well known that the subsidence inversion is enhanced during CCV HWs and plays a key role, along with suppression of the sea breeze, in HW formation (Grotjahn 2011).

Upper level convergence over lower level divergence occurs for regional sinking motion; therefore, this condition is expected near CCV during HW events. To illuminate this structure, VP fields are analyzed near the CCV when HWs develop. Figure 5 shows composites of VP anomalies for 24 CCV HW events for three days from onset at both upper (200 hPa) and lower (850 hPa) troposphere levels. Since the pressure velocity (dP/dt) is much smaller at the ground than at its mid-troposphere peak, upper and lower troposphere VP anomaly fields generally have opposite sign where VP magnitude is appreciable. This sign reversal with height is generally confirmed in most of the VP composite fields. Near the CCV (green box), a local maximum aloft and local minimum below are observed as expected, the action center is east of the CCV. However, the sign reversal with elevation is less clear in the eastern US; the upper level VP negative activity center in the eastern US does not overlie a strongly positive area. However, near southern Mexico and Central America, negative VP overlies positive VP in the lower level with similar gradient off the west coast of these lands. Outside North America, the upper tropospheric VP anomaly shows clear zonal asymmetry: divergence over the tropical eastern Indian Ocean and convergence over the central Pacific (the latter extending into the extratropics); this pattern is reversed in the lower troposphere.

For Review Only

To investigate the delayed impact by the MJO phase on the formation of a convergence over divergence vertical structure, VP fields are analyzed from anomaly composites averaged over 4 to 16 days *after* the onset of each MJO pair (Fig. 6). The horizontal pattern of VP is quite simple with a zonally-oriented dipole having convergence and divergence over the domain that is displaced eastward as the MJO shifts to higher phase numbers. The sequence of pairs in Figure 6 is roughly in quadrature: a given pair has extrema generally shifted half-way across the domain and lying in between the extrema of the immediately preceding pair. Thereby, the 6-7 (8-1) pair has VP anomaly roughly opposite to the 2-3 (4-5) pair.

The convergence over divergence vertical structure after each MJO phase pair (Fig. 6) is compared with the VP fields during HW events (Fig. 5). Figure 5 has elements of MJO pair 2-3 (Fig. 6a,c) over the Indian Ocean and Indonesia. Further east, Figure 5 has elements of 8-1 (Fig. 6f,h) over the central Pacific to Mexico. Only 2-3 and 8-1 in Figure 6 match the VP over the western US.. These roughly opposite sign and the matching elements are supported by pattern correlation coefficients of VP fields. The pattern correlations at the two levels are 0.43 (0.43), -0.95 (-0.92), -0.45 (-0.39), and 0.90 (0.81) at 200 hPa (850 hPa) for 2-3, 4-5, 6-7, and 8-1 phase pairs respectively.

The 'regional' VP field over the CCV after each MJO pair is examined next. After the phase pair 2-3, the CCV has VP>0 aloft and VP<0 below and the part at the CCV is the northern part of strong VP anomalies over the eastern Pacific. After the phase pair 8-1, the CCV also has VP>0 aloft and VP<0 below at the CCV, anomalies that are inside the eastern edge of strong VP anomalies over the central Pacific. Over the northeastern Pacific, the 8-1 VP anomaly LSMP is rapidly declines (at 200 hPa) while the corresponding 2-3 LSMP is

For Review Only

rapidly increasing (Fig. 6a,f). Similarly at 850 hPa, the 2-3 LSMP declines in the northeast Pacific while the 8-1 LSMP increases (Fig. 6c,h). So, it is not unreasonable to deduce that some combinations of these fields can create a mid-Pacific and a western US VP extrema similar to that found in Figure 5. After either of those two phase pairs, the shapes of these significant VP anomalies imply convergence over divergence at the CCV, implying sinking that would be favorable to the HW activation. Unlike Figure 5 neither phase pair has a separate VP extremum there. The VP anomaly signal over the CCV is consistent, judged by exceeding a 1/3 sign fraction value only after phase pairs 2-3 and 6-7 but not 4-5 and 8-1 (Fig. S2 in the supplementary information). Thus, convergence over divergence structure may be less robust in phase pair 8-1 compared to phase pair 2-3.

Both the larger similarity of VP LSMP and strong CCV area convergence over divergence structure support the strong association between MJO and CCV HWs. Phase pair 2-3 shows significant and consistent positive anomalies aloft and negative anomalies below in the western North America and the large scale VP pattern is similar to the field of HWs in tropical Indian Ocean pattern. After phase pair 8-1 MJO, the central Pacific VP lobe is quite similar to the HWs and significant CCV area anomalies are observed although they are less consistent than phase pair 2-3 MJO. These results indicate that both phase pairs (2-3 and 8-1) of the MJO have a connection to the CCV HWs. However, after phase pairs 4-5 and 6-7, the large scale VP pattern is reversed from the VP field during CCV HWs. Pairs 4-5 and 6-7 imply rising motion that is obviously unfavorable for adiabatic heating of air parcels, but is consistent with the cooler temperatures and smaller fraction of hot days shown in Fig. 3.

4. Distinct MJO associations between two types of CCV HWs

https://mc03.manuscriptcentral.com/aasiap

For Review Only

Prior work (LG2016) identified two different types of Californian Central Valley HWs based on their spatial and temporal development. LG2016 show that one type of HW (labelled 'Cluster 1') tends to form a strong lower tropospheric hot temperature anomaly over a region centered just offshore of the NW California and SW Oregon coasts only immediately before onset, with cold anomalies prevailing off the US NW coast several days before.. A second type of CCV HW (labelled 'Cluster 2') develops hot temperatures in that same offshore region but as a southwestward extension of a hot anomaly covering southwestern Canada that exists several days prior to the CCV HW onset. Prior sections of this article consider all HW events at once. This section considers each cluster of HW events separately and executes parallel analyses of MJO associations for each HW cluster. During the 1979-2010 period used here, there are 11 events in Cluster 1 and 9 events in Cluster 2. The remaining four events are a mixture of both cluster types.

OLR anomaly composites during three days from the HW onset date clearly show significant positive anomalies over the CCV extending to the offshore region in both clusters (Fig. 7). However, strength and spatial coverage differs between the two clusters. In Cluster 1, strong OLR>0 dominates over most of western North America, while this anomaly is shifted to the north and relatively confined to the coast in Cluster 2. The distribution of negative OLR anomalies over North America is distinct in the two clusters. In Cluster 1, negative anomalies are mainly located in Mexico, Texas, and the Midwest. In Cluster 2, however, they are situated further south from offshore of southwestern Mexico across the Gulf of Mexico and extending along the US east coast. The pairing of negative (ascending) anomalies to the south and positive (descending) anomalies to the north suggests that the Matsuno-Gill model may be applicable at least during days after HW

For Review Only

events onset in both clusters as mentioned before. However, the enhanced convection (implied by the OLR anomalies) in Cluster 1 is mostly over the land surface not over the eastern Pacific Ocean surface while much of the Cluster 2 OLR<0 LSMP is over water. The meridional scale of a circulation from southern convection to north-northwest subsidence is smaller in Cluster 1 compared to Cluster 2.

VP anomaly composites for three days from HW onset are displayed for two clusters and they are compared for upper and lower tropospheric levels in Figure 8. Cluster 1 shows very clear and significant patterns of negative anomalies to the west (tropical Indian Ocean) and positive anomalies to the east (central North Pacific) at 200 hPa with the pattern largely reversing sign at 850 hPa (Fig. 8a,b). The Cluster 1 pattern visually matches the MJO phase pair 8-1 composite pattern (Fig. 6) better than other phase pairs. The Cluster 2 VP anomaly composites at 200 hPa are weaker than in Cluster 1 in both positive and negative anomaly cells, while negative anomalies at 850 hPa are stronger than in Cluster 1. In addition, the positive anomaly cell aloft and negative anomaly cell below are displaced to the western Pacific. The pattern of Cluster 2 looks generally similar to the MJO phase pair 8-1 composite pattern (Fig. 6f,h) but less similar than Cluster 1 does.

The details near the CCV for the two clusters are noteworthy. Cluster 1 has significant, localized, strong VP>0 anomaly over strong VP<0 anomaly over western North America. In Cluster 2, however, the VP vertical structure is weak and insignificant there. Close inspection of Cluster 2 finds at the 850hPa level: a significant VP minimum off the British Columbia and Washington coast and a VP ridge centered to the southeast, extending to Mexico. The pattern for Cluster 2 in Figure 8e implies sinking off the British Columbia and Washington coasts that is consistent with the OLR fields during HW onset (Fig. 7b) as

https://mc03.manuscriptcentral.com/aasiap

For Review Only

well as the pre-existing HW in SW Canada at the time of Cluster 2 HW onset (shown in LG2016).

The MJO phase pair associations with the two HW clusters is quantitatively assessed using pattern correlations of VP fields (Figs. 8c,f). Both Cluster 1 and 2 composites show largest pattern correlations with phase pair 8-1, consistent with the description above. A major difference between the two clusters is that in Cluster 2 the correlations for all four phase pairs are smaller in magnitude than corresponding correlations in Cluster 1. Notably, the pattern correlation for phase pair 2-3 is negligibly small for Cluster 2 but not for Cluster 1. The pattern of VP, especially the westward shifted North Pacific anomalies, is out of phase with the pattern of the 2-3 phase pairs therefore the correlation for the 2-3 pair field is much less with Cluster 2. From results in Figures 7 and 8, it is deduced that Cluster 2 CCV HWs are less well associated with leading MJO convections but, to the extent they are associated, they are more linked to phase pair 8-1 (eastern Pacific) convection than other phase pairs.

5. Discussion and Summary

In prior works (Grotjahn and Faure, 2008; Grotjahn, 2011; Lee and Grotjahn, 2016), LSMPs in the subtropical, middle, and high latitudes were identified that are associated with CCV HWs. This study explores the tropical MJO connection to CCV HWs by comparing LSMPs during the HWs and after the MJO convection. The associations are tracked for different longitudinal locations of the tropical convection in terms of MJO RMM index phase pairs. The MJO in summertime is characterized not only by eastward migration of a region of tropical convection but also by northward propagation and expansion of the convective

For Review Only

region as it approaches the eastern Pacific, a pattern that is generally seen from OLR anomaly composites. OLR anomaly composites prior to CCV HWs look like a combination of the Indian Ocean (MJO 2-3 phase pair) and the eastern Pacific (MJO 8-1 phase pair) convection patterns (Fig. 2). In addition, those two phase pairs are more frequently active prior to HWs compared to the other two phase pairs. The fact that the CCV HWs are preceded by specific phases of MJO convection prompted this research.

One would not expect distant tropical convection to immediately affect the CCV. The average time taken to affect the CCV is estimated from time series of the mean normalized temperature anomalies at CCV stations and the fraction of 5% hot days after each MJO event onset (Fig. 3). Those two temperature metrics show that the timing of hot weather after MJO events differs among the four phase pairs: earlier activation and sooner decay for phase pair 8-1, later activation for phase pair 2-3. Also evident is the activation of the cooler temperatures for phase pairs 4-5 and 6-7. By synthesizing the results of two temperature extreme metrics, the time periods of 4 to 16 days after an MJO events onset was chosen. Two temperature extreme metrics averaged during that time period indicate that CCV HWs are the most strongly connected to eastern Pacific MJO convection (phase pair 8-1), and secondarily connected to Indian Ocean MJO convection (phase pair 2-3). HWs are least connected to Maritime Continent MJO convection (phase pair 4-5).

The LSMP of OLR after 4 to 16 days after MJO events onset (Fig. 4) clearly displays eastward and northward displaced pattern of the typical summertime MJO convection for four individual phase pairs. OLR is used as a proxy for vertical motions. In far distant, extratropical, western North America, apparent subsidence is detected only after phase pairs 2-3 and 8-1 and not after phase pairs 4-5 and 6-7.

For Review Only

VP anomaly fields after MJO phase pairs are examined on two pressure levels (200 hPa and 850 hPa) in association with CCV HWs. The Laplacian of VP is the divergence, so VP anomalies could be interpreted in terms of general areas of divergence (VP<0) and convergence (VP>0). VP sign reversal with height occurs in areas of enhanced upward or downward motion anomaly. As expected, localized convergence over divergence feature occurs over the western US during three-day periods beginning with each HW onset. The LSMP of VP anomaly at both levels shows clear zonal asymmetry with divergence over convergence to the west (tropical Indian Ocean) and convergence over divergence to the east of approximately 120°E (western to central North Pacific) (Fig. 5). When compared to this pattern, VP anomaly fields after MJO phase pairs 2-3 and 8-1 (Fig. 6) each match specific parts. In addition, part of VP LSMP extending to the eastern North Pacific after these two phase pairs is favorable to the formation of CCV HWs: enhanced convergence over divergence there. These MJO lagged composites indicate robust associations between CCV HWs and specific MJO phases and they are consistent with the MJO phase dependencies deduced from temperature extreme metrics; the CCV hot weather is most common after the eastern Pacific MJO, and next most common after Indian Ocean MJO phases.

The MJO connections to the two types of CCV HWs are examined by making parallel comparisons to those done for all HWs. Both clusters have strong subsidence in the eastern North Pacific paired with significant enhanced convection to the south-southeast. . Cooler temperatures and higher sea level pressure off the California coast have been linked to increased OLR values in Central America and across the equator (Grotjahn and Osman, 2007) as well as opposite signs for these features. However, the pattern appears to be a

https://mc03.manuscriptcentral.com/aasiap

For Review Only

stronger Matsuno-Gill model response in Cluster 2 than Cluster 1. VP anomalies at zero to two days after CCV HW onset reveal additional differences between the two cluster types. One notable difference occurs over the CCV: much weaker magnitude of the VP anomaly in Cluster 2 compared to Cluster 1, implying upper level convergence and lower level divergence in situ is less prominent during Cluster 2 HWs. Another difference is the convergence over divergence structure over the Pacific is shifted far westward for Cluster 2. Consequently, the LSMP has less consistency with VP fields formed from lagging MJO phase pairs except phase pair 8-1. Therefore, Cluster 2 has less association with the MJO and is only evident after phase pair 8-1.

The midlatitude Rossby wave source is usually strong at the polar-side of tropical convection leading to upper level extratropical convergence that then generates transient waves that propagate eastward (Tyrrell et al. 1996). Individual VP anomaly fields show that an eastward propagating wave signal is usually present before HW onset in both clusters (not shown). This may be partly associated with MJOs although in the anomaly pattern it is hard to isolate solely a tropics-originated signal from intrinsic subtropical transient waves. A wavy pattern in extratropical VP fields is more clearly visible in Cluster 1 than in Cluster 2 with shorter wavelength in Cluster 1 (Fig. 8). These features are consistent with geopotential height composite fields shown in LG2016.

It is challenging to isolate clearly the contributions of tropical convection in different longitudinal locations (that is, the contribution of different MJO phases) to phenomena in a remote subtropical region. For instance, CCV hot weather activity after phase MJO pair 2-3 could be partly contaminated by other subsequent phase pairs given the distance between the atmospheric phenomena. However, this study mitigates that

For Review Only

interference by focusing upon substantially strong MJO events. In addition, this study does not seek to prove the connections between the MJO phases and the CCV HWs, but to discover associations that can motivate further study of the connections.

Acknowledgements

This research was funded in part by NSF Grant 1236681, Department of Energy Office of Science award number DE-SC0016605, and by the USDA National Institute of Food and Agriculture, Hatch project Accession #1010971. This research was also supported by the APEC Climate Center in Republic of Korea.

References

Alexander, L. V., P. Uotila, and N. Nicholls, 2009: Influence of sea surface temperature variability on global temperature and precipitation extremes. *J. Geophys. Res.: Atmos.* **114**, D18116, doi:10.1029/2009JD012301.

Brown, S., J. Caesar, and C. A. Ferro, 2008: Global changes in extreme daily temperature since 1950. *J. Geophys. Res.: Atmos.* **113**, D05115, doi: 10.1029/2006JD008091.

Cellitti, M. P., J. E. Walsh, R. M. Rauber, and D. H. Portis, 2006: Extreme cold air outbreaks over the United States, the polar vortex, and the large-scale circulation. *J. Geophys. Res.: Atmos.* **111**, D02114, doi:10.1029/2005JD006273.

Dee, D. P., Uppala, S. M., Simmons, A. J., Berrisford, P. , Poli, P. , Kobayashi, S., et al. , 2011: The ERA-Interim reanalysis: configuration and performance of the data assimilation system. *Quart. J. Roy. Meteorol. Soc.,* **137,** 553-597. doi:10.1002/qj.828

For Review Only

Downton, M. W., and K. A. Miller, 1993: The freeze risk to Florida citrus. Part II: Temperature variability and circulation patterns. *J. Climate*, **6,** 364-372. doi: 10.1175/1520-0442(1993)006<0364:TFRTFC>2.0.CO;2

Gershunov, A., D. R. Cayan, and S. F. Iacobellis, 2009: The great 2006 heat wave over California and Nevada: Signal of an increasing trend. *J. Climate*, **22,** 6181-6203. doi: 10.1175/2009JCLI2465.1

Gill, A. E., 1980: Some simple solutions for heat-induced tropical circulation. *Quart. J. Roy. Meteorol. Soc.,* **106,** 447-462. doi:10.1002/qj.49710644905

Grotjahn, R., 2011: Identifying extreme hottest days from large scale upper air data: a pilot scheme to find California Central Valley summertime maximum surface temperatures. *Clim. Dyn.*, **37,** 587-604. doi: 10.1007/s00382-011-0999-z

Grotjahn, R., 2013: Ability of CCSM4 to simulate California extreme heat conditions from evaluating simulations of the associated large scale upper air pattern. *Clim. Dyn.*, **41,** 1187-1197. doi: 10.1007/s00382-013-1668-1

Grotjahn, R., R., 2016: Western North American Extreme heat, associated large scale synoptic-dynamics, and performance by a climate model. *Dynamics and predictability of large-scale, high-impact weather and climate events*, edited by J. Li et al., Cambridge University Press, Cambridge. 198-209. ISBN: 9781107071421.

Grotjahn, R., and M. Osman, 2007: Remote weather associated with North Pacific subtropical sea level high properties. *Int'l J. Climatol.*, **27,** 587-602. doi: 10.1002/joc.1423

For Review Only

Grotjahn, R., and G. Faure, 2008: Composite predictor maps of extraordinary weather events in the Sacramento, California, Region. *Wea. and Forecast.*, **23,** 313-335. doi: 10.1175/2007WAF2006055.1

Grotjahn, R., and Coauthors, 2016: North American extreme temperature events and related large scale meteorological patterns: a review of statistical methods, dynamics, modeling, and trends. *Clim. Dyn.*, **46,** 1151-1184. doi: 10.1007/s00382-015-2638-6

Guirguis, K., A. Gershunov, R. Schwartz, and S. Bennett, 2011: Recent warm and cold daily winter temperature extremes in the Northern Hemisphere. *Geophys. Res. Lett.*, **38**, L17701. doi: 10.1029/2011GL048762

Higgins, R. W., and K. C. Mo, 1997: Persistent North Pacific circulation anomalies and the tropical intraseasonal oscillation. *J. Climate*, **10,** 223-244. doi: 10.1175/1520-0442(1997)010<0223:PNPCAA>2.0.CO;2

Higgins, R. W., A. Leetmaa, and V. E. Kousky, 2002: Relationships between climate variability and winter temperature extremes in the United States. *J. Climate*, **15,** 1555-1572. doi: 10.1175/1520-0442(2002)015<1555:RBCVAW>2.0.CO;2

Hong, C.-C., and T. Li, 2009: The extreme cold anomaly over Southeast Asia in february 2008: Roles of ISO and ENSO. *J. Climate*, **22,** 3786-3801. doi: 10.1175/2009JCLI2864.1

Hoskins, B., 1996: On the existence and strength of the summer subtropical anticyclones: Bernhard Haurwitz memorial lecture. *Bull. Amer. Meteorol. Soc.*, **77,** 1287-1292.

Hoskins, B., R. Neale, M. Rodwell, and G.-Y. Yang, 1999: Aspects of the large-scale tropical atmospheric circulation. *Tellus B*, **51,** 33-44. doi:10.1034/j.1600-0889.1999.00004.x

For Review Only

Jeong, J.-H., C.-H. Ho, B.-M. Kim, and W.-T. Kwon, 2005: Influence of the Madden-Julian Oscillation on wintertime surface air temperature and cold surges in east Asia. *J. Geophys. Res.: Atmos.* **110,** D11104, doi:10.1029/2004JD005408.

Jeong, J.-H., B.-M. Kim, C.-H. Ho, and Y.-H. Noh, 2008: Systematic variation in wintertime precipitation in East Asia by MJO-induced extratropical vertical motion. *J. Climate*, **21,** 788-801. doi: 10.1175/2007JCLI1801.1

Jin, F., and B. Hoskins, 1995: The direct response to tropical heating in a baroclinic atmosphere. *J. Atmos. Sci.*, **52,** 307-319. doi: 10.1175/1520-0469(1995)052<0307:TDRTTH>2.0.CO;2

Jones, C., J. Gottschalck, L. M. V. Carvalho, and W. Higgins, 2010: Influence of the Madden–Julian Oscillation on forecasts of extreme precipitation in the contiguous United States. *Mon. Wea. Rev.*, **139,** 332-350, doi: 10.1175/2010MWR3512.1

Kenyon, J., and G. C. Hegerl, 2008: Influence of modes of climate variability on global temperature extremes. *J. Climate*, **21,** 3872-3889, doi: 10.1175/2008JCLI2125.1

Kiladis, G. N., and K. M. Weickmann, 1992: Circulation anomalies associated with tropical convection during northern winter. *Mon. Wea. Rev.*, **120,** 1900-1923. doi: 10.1175/1520-0493(1992)120<1900:CAAWTC>2.0.CO;2

Kiladis, G.N., J. Dias, K.H. Straub, M.C. Wheeler, S.N. Tulich, K. Kikuchi, K.M. Weickmann, and M.J. Ventrice, 2014: A Comparison of OLR and Circulation-Based Indices for Tracking the MJO. Mon. Wea. Rev., 142, 1697–1715, https://doi.org/10.1175/MWR-D-13-00301.1

For Review Only

Lau, K.-M., and T. J. Phillips, 1986: Coherent fluctuations of extratropical geopotential height and tropical convection in intraseasonal time scales. *J. Atmos. Sci.*, **43,** 1164-1181. doi: 10.1175/1520-0469(1986)043<1164:CFOFGH>2.0.CO;2

Lee, H.-T., A. Gruber, R. G. Ellingson, and I. Laszlo, 2007: Development of the HIRS outgoing longwave radiation climate dataset. *J. Atmos. and Oceanic Tech.*, **24,** 2029-2047. doi: 10.1175/2007JTECHA989.1

Lee, Y.-Y., and R. X. Black, 2013: Boreal winter low-frequency variability in CMIP5 models. *J. Geophys. Res.: Atmos.* **118,** 6891-6904. doi: 10.1002/jgrd.50493.

Lee, Y. Y., and R. Grotjahn, 2016: California Central Valley summer heat waves form two ways. *J. Climate,* **29**, 1201-1217. doi: 10.1175/JCLI-D-15-0270.1

Lim, Y. K., and S. D. Schubert, 2011: The impact of ENSO and the Arctic Oscillation on winter temperature extremes in the southeast United States. *Geophys. Res. Lett.*, **38**. L15706, doi:10.1029/2011GL048283.

Lin, H., and G. Brunet, 2009: The influence of the Madden–Julian Oscillation on Canadian wintertime surface air temperature. *Mon. Wea. Rev.*, **137,** 2250-2262. doi: 10.1175/2009MWR2831.1

Lin, H., G. Brunet, and J. Derome, 2009: An observed connection between the North Atlantic Oscillation and the Madden–Julian Oscillation. *J. Climate*, **22,** 364-380. doi: 10.1175/2008JCLI2515.1

Lin, H., G. Brunet, and R. Mo, 2010: Impact of the Madden–Julian Oscillation on wintertime precipitation in Canada. *Mon. Wea. Rev.*, **138,** 3822-3839. doi: 10.1175/2010MWR3363.1

For Review Only

Loikith, P. C., and A. J. Broccoli, 2014: The influence of recurrent modes of climate variability on the occurrence of winter and summer extreme temperatures over North America. *J. Climate*, **27,** 1600-1618. doi: 10.1175/JCLI-D-13-00068.1

Madden, R., and P. Julian, 1994: Observations of the 40-50-day tropical oscillation-A review. *Mon. Wea. Rev.*, **122,** 814-837. doi: 10.1175/1520-0493(1994)122<0814:OOTDTO>2.0.CO;2

Madden, R. A., and P. R. Julian, 1972: Description of global-scale circulation cells in the tropics with a 40–50 day period. *J. Atmos. Sci.*, **29,** 1109-1123. doi: 10.1175/1520-0469(1972)029<1109:DOGSCC>2.0.CO;2

Matsueda, S., and Y. Takaya, 2015: The global influence of the Madden–Julian Oscillation on extreme temperature events. *J. Climate*, **28,** 4141-4151. doi: 10.1175/JCLI-D-14-00625.1

Matsuno, T., 1966: Quasi-geostrophic motions in the equatorial area. *J. Meteorol. Soc. Japan*, Ser. II, **44,** 25-43. doi: 10.2151/jmsj1965.44.1_25

Matthews, A. J., B. J. Hoskins, and M. Masutani, 2004: The global response to tropical heating in the Madden–Julian oscillation during the northern winter. *Quart. J. Roy. Meteorol. Soc.* **130,** 1991-2011. doi:10.1256/qj.02.123

Meehl, G., and H. Teng, 2007: Multi-model changes in El Nino teleconnections over North America in a future warmer climate. *Clim. Dyn.*, **29,** 779-790. doi: 10.1007/s00382-007-0268-3

Moon, J.-Y., B. Wang, and K.-J. Ha, 2011: ENSO regulation of MJO teleconnection. *Clim. Dyn.*, **37,** 1133-1149. doi: 10.1007/s00382-010-0902-3

For Review Only

Mori, M., and M. Watanabe, 2008: The growth and triggering mechanisms of the PNA: A MJO-PNA coherence. *J. Meteorol. Soc. Japan. Ser. II*, **86,** 213-236. doi: 10.2151/jmsj.86.213

Palipane, E., and R. Grotjahn, 2018: Future projections of the large-scale meteorology associated with California heat waves in CMIP5 models. *J. Geophys. Res.: Atmos.* **123,** 8500-8517. doi: 10.1029/2018JD029000.

Schreck, C. J., J. M. Cordeira, and D. Margolin, 2013: Which MJO events affect North American temperatures? *Mon. Wea. Rev.*, **141,** 3840-3850. doi: 10.1175/MWR-D-13-00118.1

Sillmann, J., M. Croci-Maspoli, M. Kallache, and R. W. Katz, 2011: Extreme cold winter temperatures in Europe under the influence of North Atlantic atmospheric blocking. *J. Climate*, **24,** 5899-5913. doi: 10.1175/2011JCLI4075.1

Tyrrell, G., D. Karoly, and J. McBride, 1996: Links between tropical convection and variations of the extratropical circulation during TOGA COARE. *J. Atmos. Sci.*, **53,** 2735-2748. doi: 10.1175/1520-0469(1996)053<2735:LBTCAV>2.0.CO;2

Walsh, J. E., A. S. Phillips, D. H. Portis, and W. L. Chapman, 2001: Extreme cold outbreaks in the United States and Europe, 1948-99. *J. Climate*, **14,** 2642-2658. doi: 10.1175/1520-0442(2001)014<2642:ECOITU>2.0.CO;2

Wang, S., Ma, D., Sobel, A.H. and Tippett, M.K., 2018. Propagation characteristics of BSISO indices. Geophysical Research Letters, 45(18), pp.9934-9943.

Wettstein, J. J., and L. O. Mearns, 2002: The influence of the North Atlantic–Arctic Oscillation on mean, variance, and extremes of temperature in the Northeastern United States

For Review Only

and Canada. *J. Climate*, **15,** 3586-3600. doi: 10.1175/1520-0442(2002)015<3586:TIOTNA>2.0.CO;2

Wheeler, M., and H. Hendon, 2004: An all-season real-time multivariate MJO index: Development of an index for monitoring and prediction. *Mon. Wea. Rev.*, **132,** 1917–1932. doi: 10.1175/1520-0493(2004)132<1917:AARMMI>2.0.CO;2

Wheeler, M. C., H. H. Hendon, S. Cleland, H. Meinke, and A. Donald, 2009: Impacts of the Madden–Julian Oscillation on Australian rainfall and circulation. *J. Climate*, **22,** 1482-1498. doi: 10.1175/2008JCLI2595.1

Zhang, C., 2005: Madden-julian oscillation. *Reviews of Geophysics*, **43**, RG2003, doi: 10.1029/2004RG000158.

Zhou, S., M. L'Heureux, S. Weaver, and A. Kumar, 2012: A composite study of the MJO influence on the surface air temperature and precipitation over the continental United States. *Clim. Dyn.*, **38,** 1459-1471. doi: 10.1007/s00382-011-1001-9

For Review Only

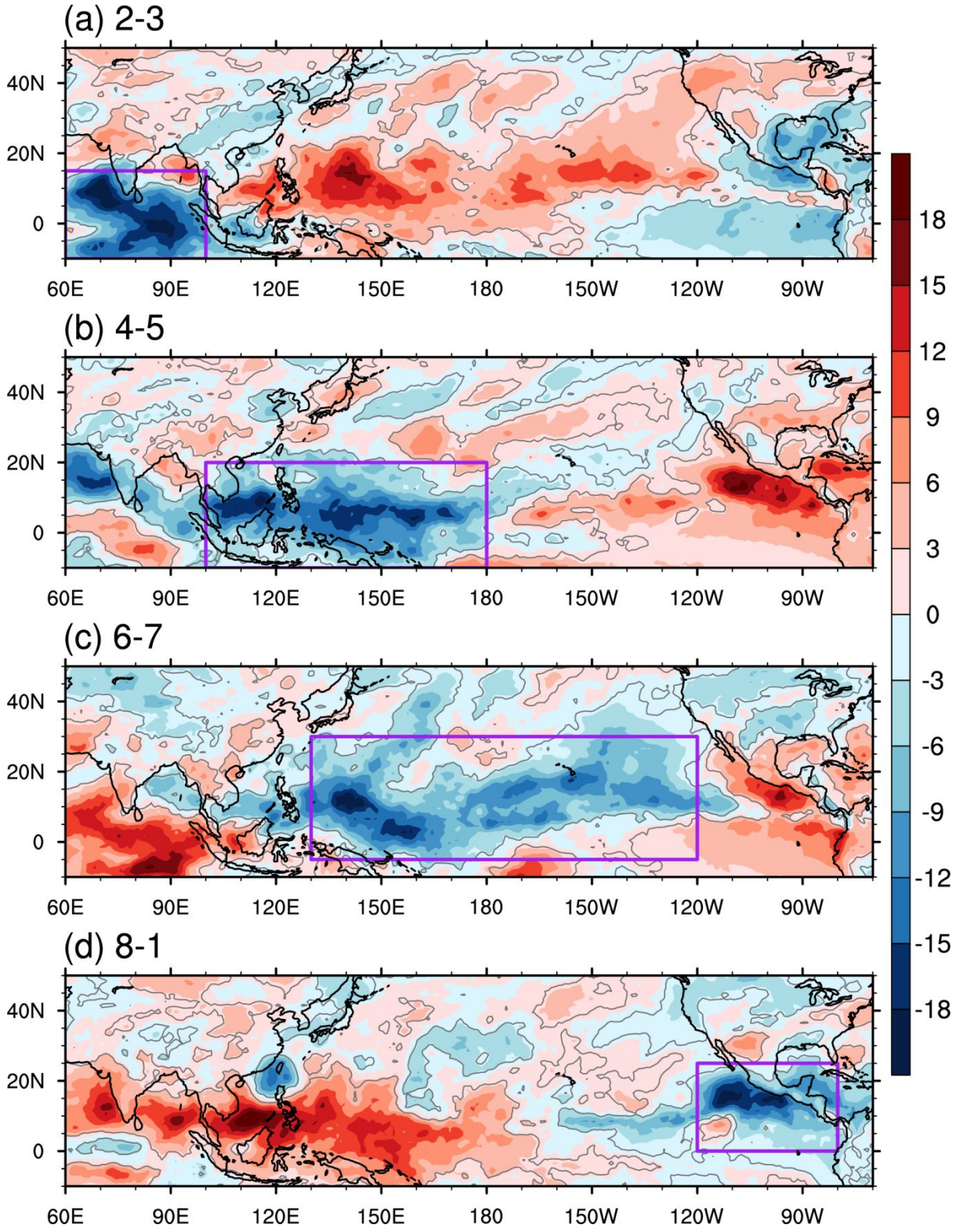

Figure 1. OLR anomaly composites from MJO events onset date for four MJO phase pairs during 1979-2010 summer seasons. An MJO event must last at least three days, have RMM≥1, and be separated ≥10 days from another event. The unit of shading is Wm^{-2}. Areas enclosed with grey contours are significant at the 95% confidence level according to the two-tailed student's t-test. Purple boxes show areas of larger OLR magnitude for each MJO phase pair.

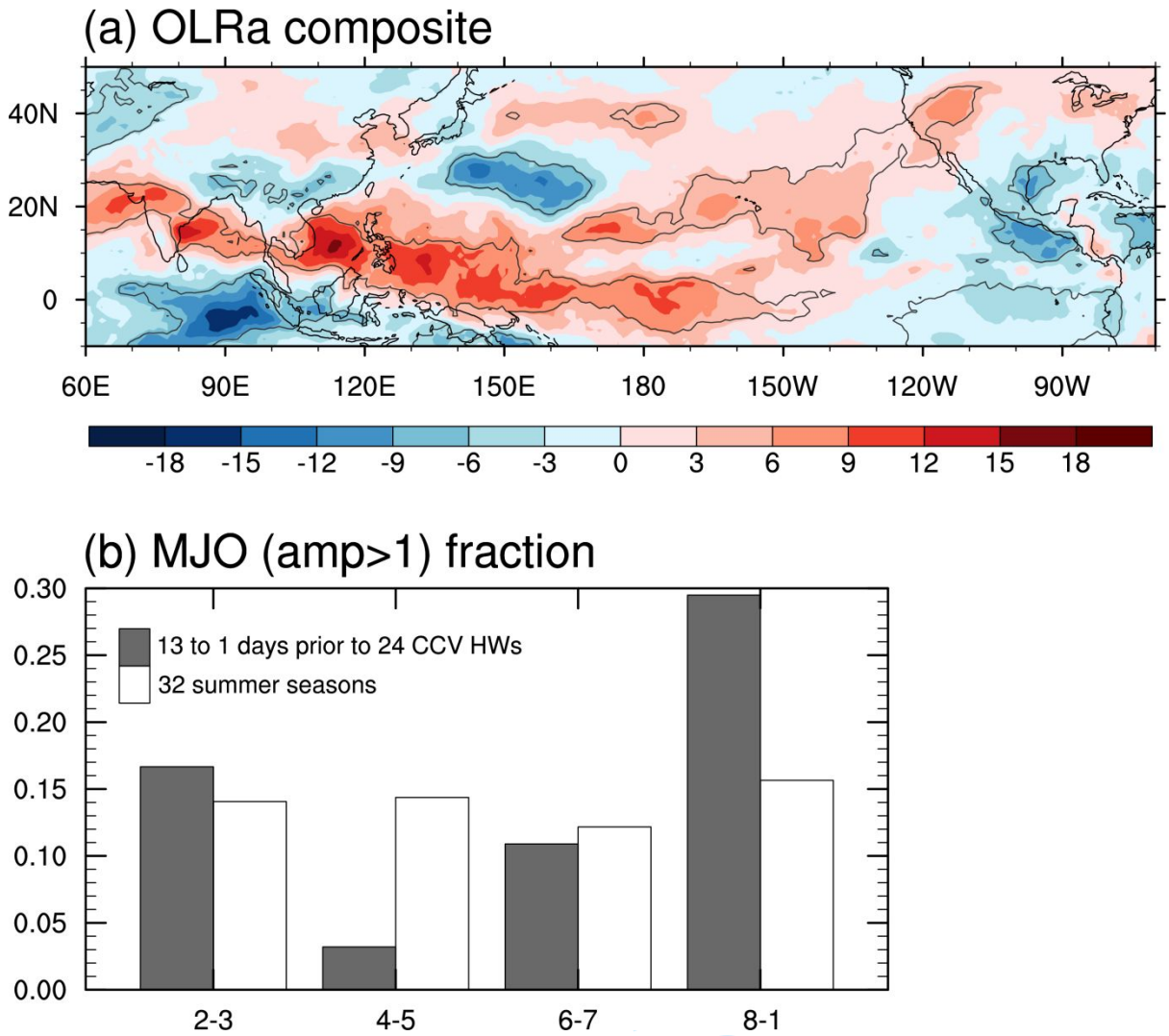

Figure 2. (a) OLR anomaly composite during the 13 days prior to 24 CCV HW events onset. The unit of shading is Wm^{-2}. Areas enclosed with grey contours are significant at the 95% confidence level according to the two-tailed student's t-test. (b) Fraction of active MJO days with RMM amplitde ≥1 for each of four phase pairs out of (dark grey) 13 days prior to all 24 HW onset dates and among (light grey) all 32 seasons of summer days.

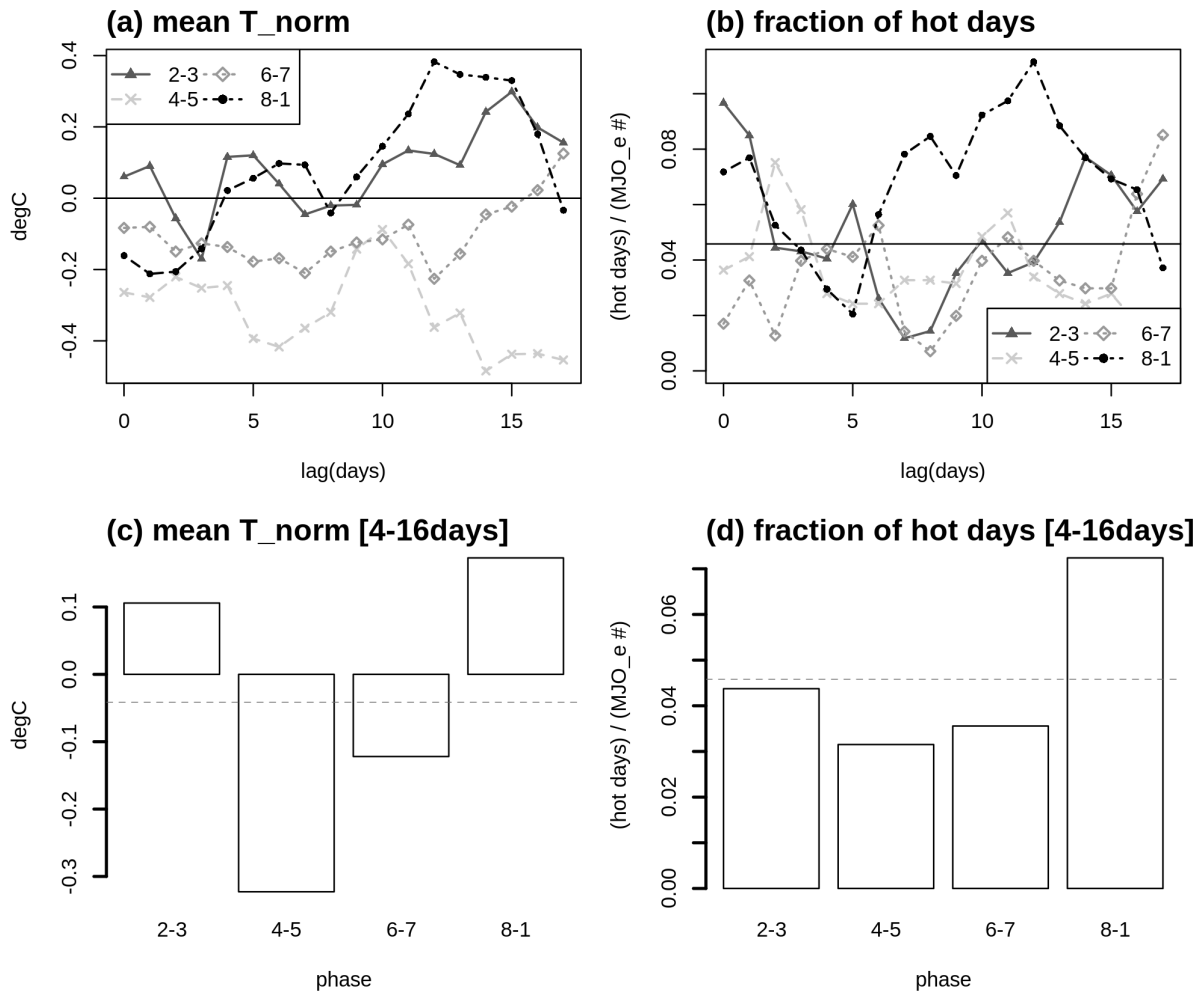

Figure 3. Temporal evolution of (a) mean normalized temperature anomalies and (b) fraction of hot days averaged over 15 CCV stations after MJO events onset during four phase pairs. Lag 1 is the day following the onset date of each individual MJO event. The average of (a) and (b) for 4-16 lag days are shown in (c) and (d). Horizontal dashed line denotes the average of four phase pairs in (c) and (d).

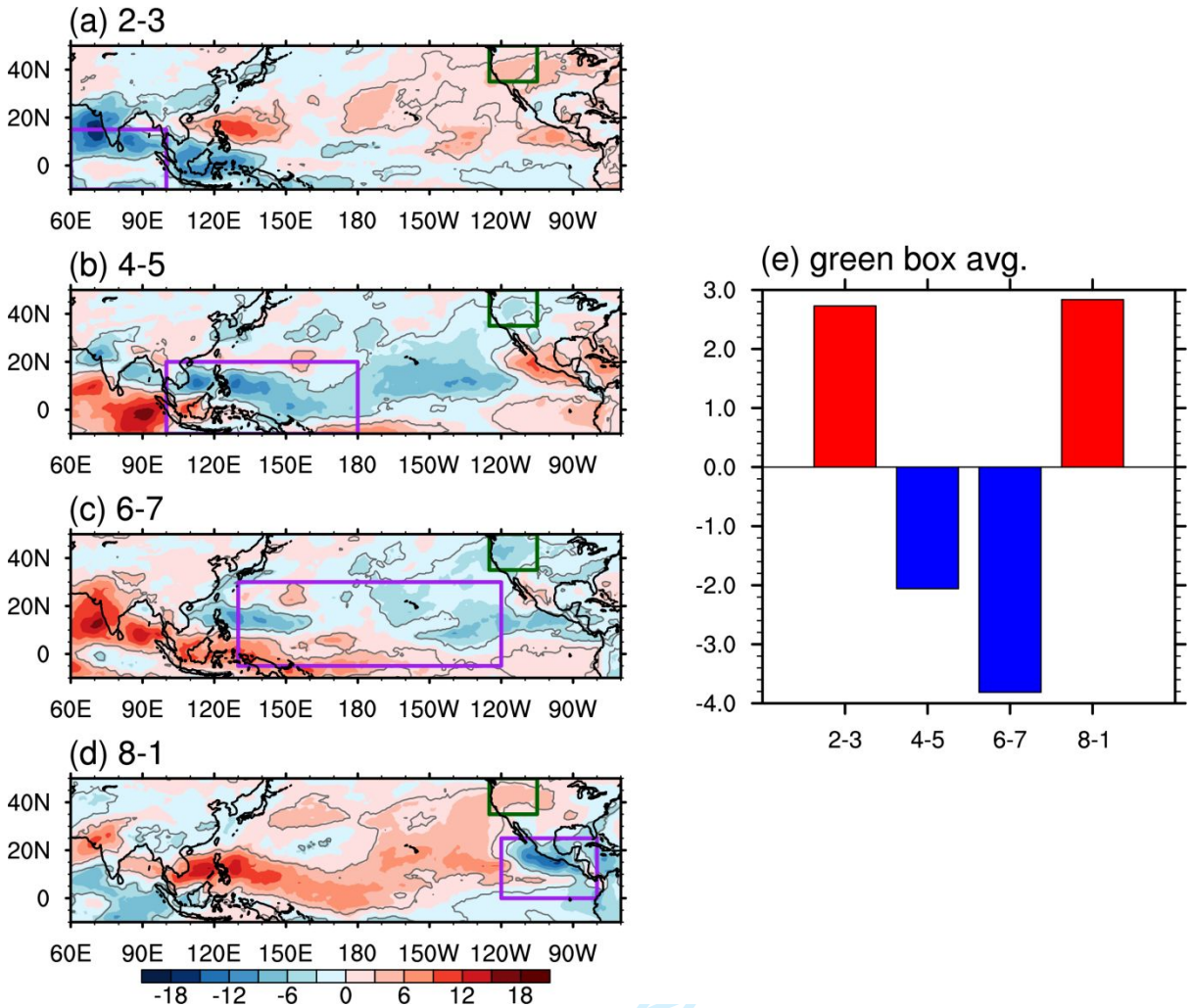

Figure 4. (a-d) OLR anomaly composites of 4-16 days after all MJO events onset dates and (e) area averaged OLR anomalies over the green boxed area for each of four phase pairs. Areas enclosed with grey contours in (a-d) are significant at the 95% confidence level according to the two-tailed student's t-test. Purple boxes show areas of larger OLR magnitude in corresponding phase pairs (shown in Figure 1). The green box shows an area of larger OLR magnitude near the CCV (125°W-105°W, 35°N-50°N).

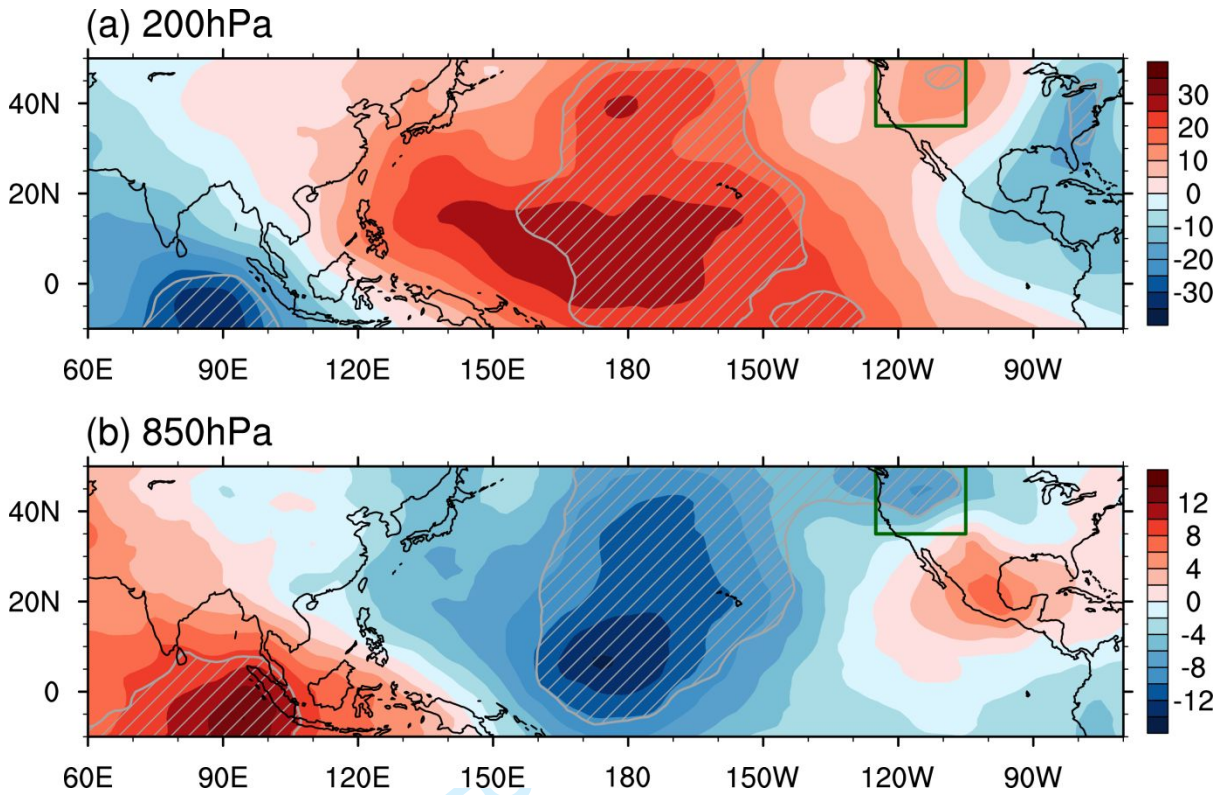

Figure 5. VP anomaly composites from all 24 CCV HW events onset for (a) 200 hPa and (b) 850 hPa. The unit of shading is 10^5 m^2s^{-1}. Hatched areas enclosed with contours are significant at the 95% confidence level according to the two-tailed student's t-test.

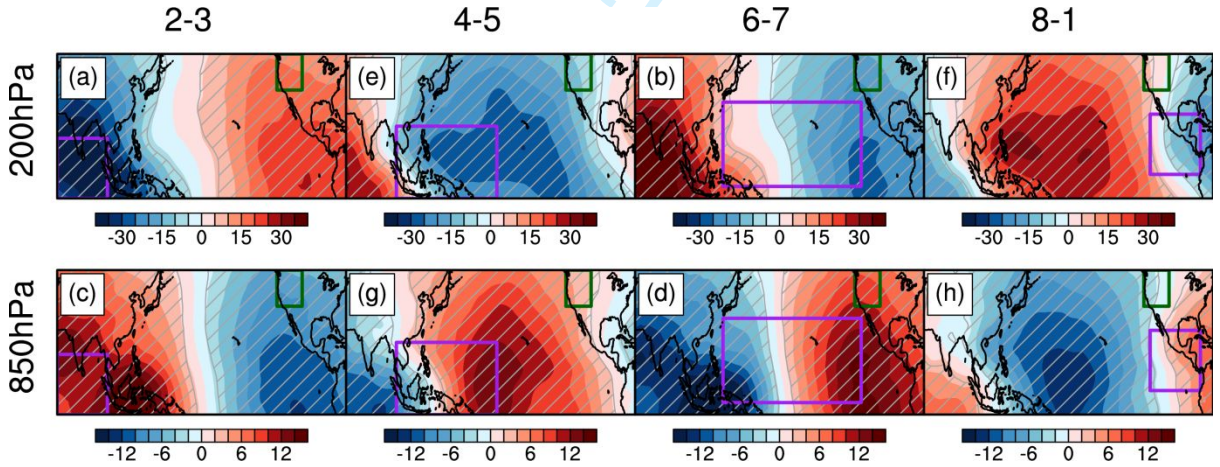

Figure 6. VP anomaly composites of 4-16 days after all MJO events onset date for four phase pairs at (a,e,b,f) 200 hPa and (c,g,d,h) 850 hPa. The unit of shading is 10^5 m^2s^{-1}. Hatched areas enclosed with contours are significant at the 95% confidence level according to the two-tailed student's t-test. Purple boxes show areas of larger OLR magnitude in corresponding phase pairs (as in Figure 1).

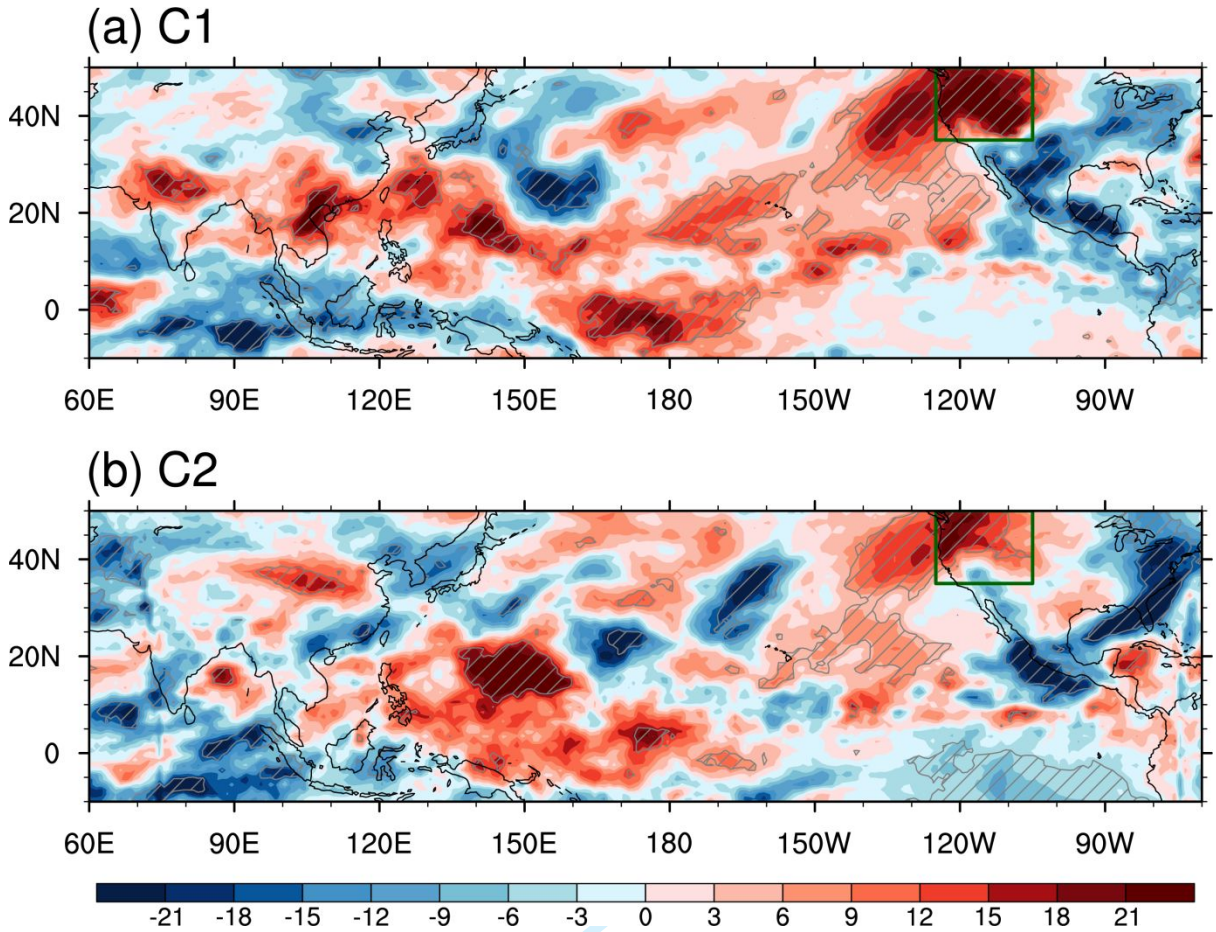

Figure 7. OLR anomaly composites during 3 days from CCV HW events onset for (a) Custer 1 and (b) Cluster 2. The unit of shading is Wm^{-2}. Hatched areas enclosed with contours are significant at the 95% confidence level according to the two-tailed student's t-test.

iew Only

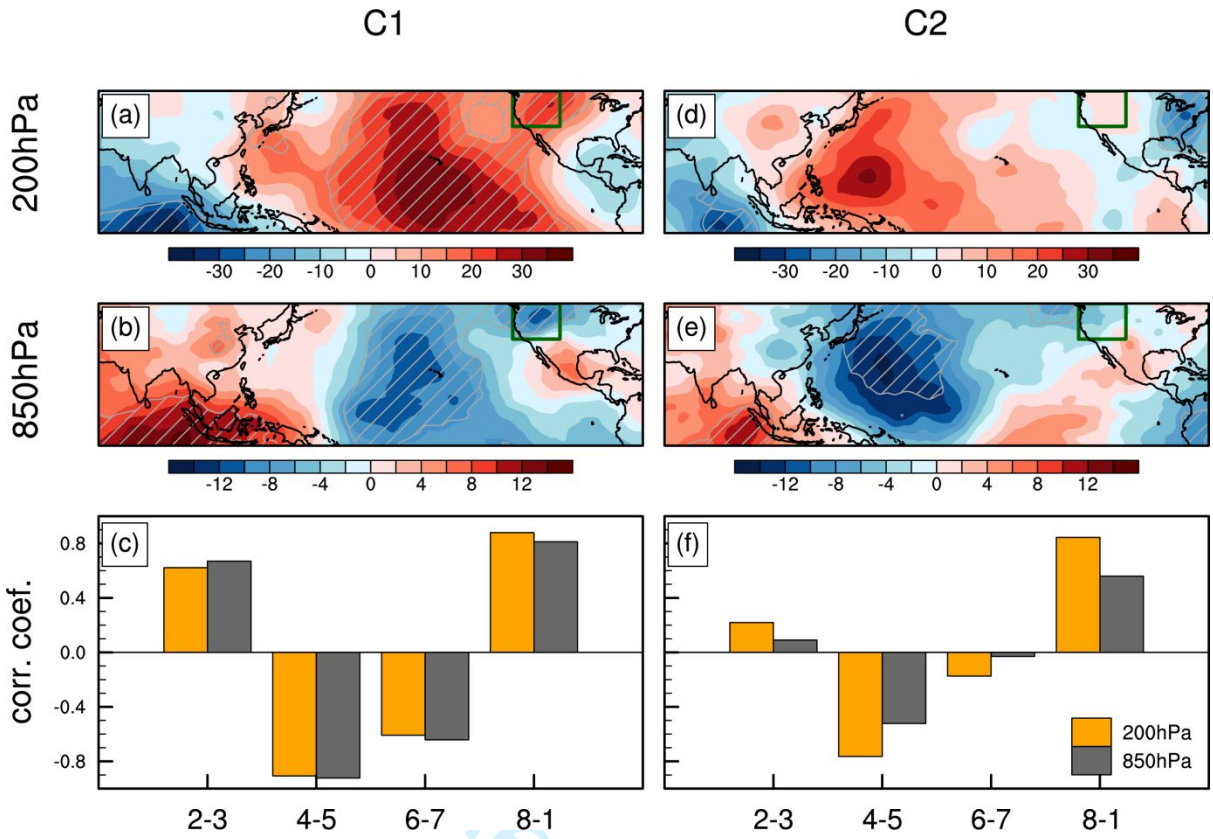

Figure 8. VP anomaly composites during 3 days from CCV HW events onset similar to Figure 5 but for each of two clusters at (a, d) 200 hPa and (b, e) 850 hPa. The unit of shading is 10^5 m^2s^{-1}. Hatched areas enclosed with contours are significant at the 95% confidence level according to the two-tailed student's t-test. Bars in (c,f) show pattern correlation coefficients between individual VP field of two CCV HW clusters (a,b,d,e) and the VP field during 4-16 days after MJO events for each of four phase pairs (shown in Figure 6) over the whole domain (60°E-70°W, 10°S-50°N). Orange and dark gray bars are for 200 hPa and 850 hPa, respectively.

Review Only

Supporting information for

Evidence of Specific MJO Phase Occurrence with Summertime California Central Valley Extreme Hot Weather

Yun-Young Lee[1] and Richard Grotjahn[2]

[1]*APEC Climate Center, Busan, South Korea*

[2]*Department of Land, Air and Water Resources, University of California, USA*

Advances in Atmospheric Science

January 2019

For Review Only

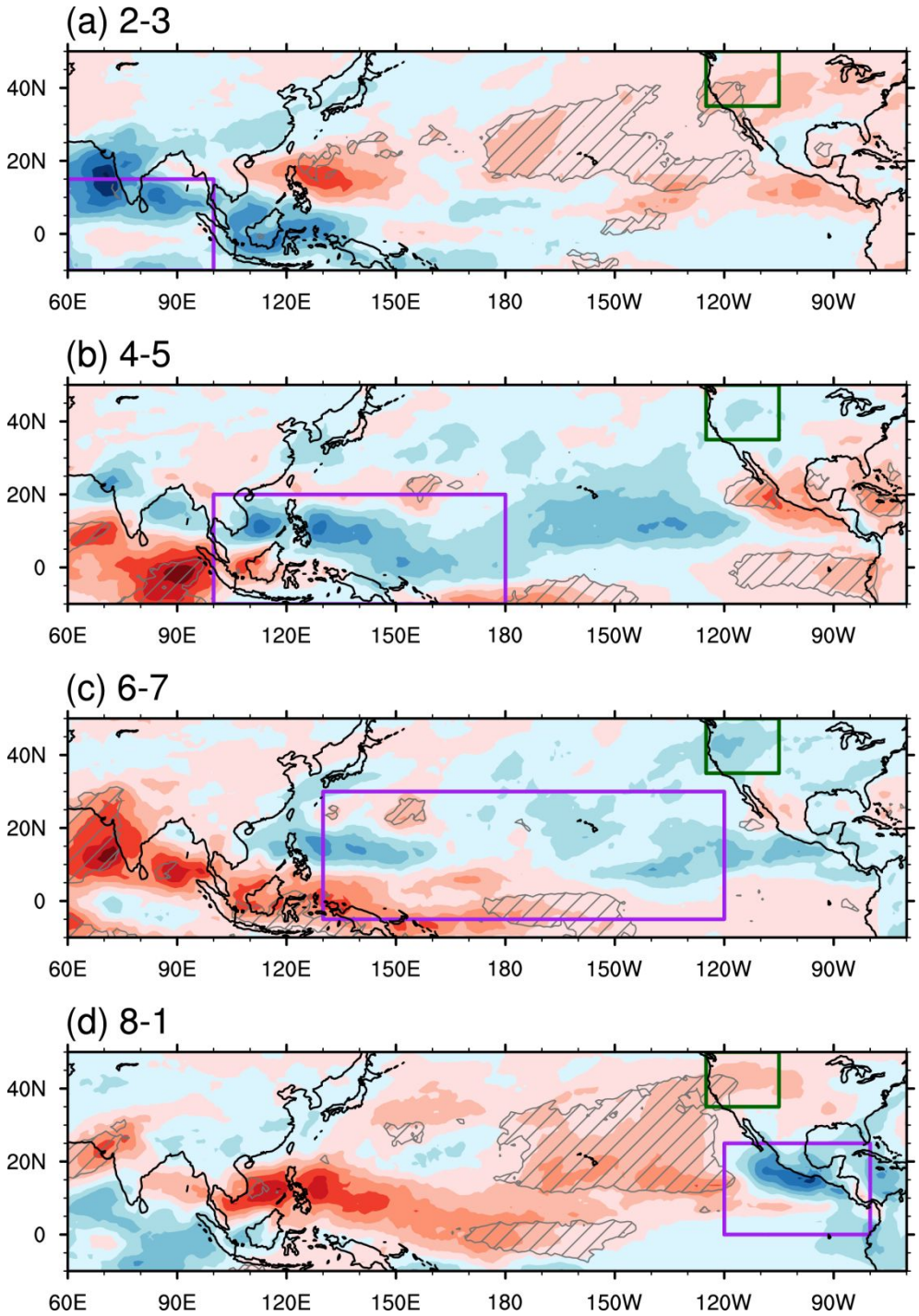

Figure S1. Same as Fig. 4(a-d) in the manuscript but gray hatching enclosed with contours displays the regions where at least two thirds of sample days have the same sign (either plus or minus) OLR anomalies.

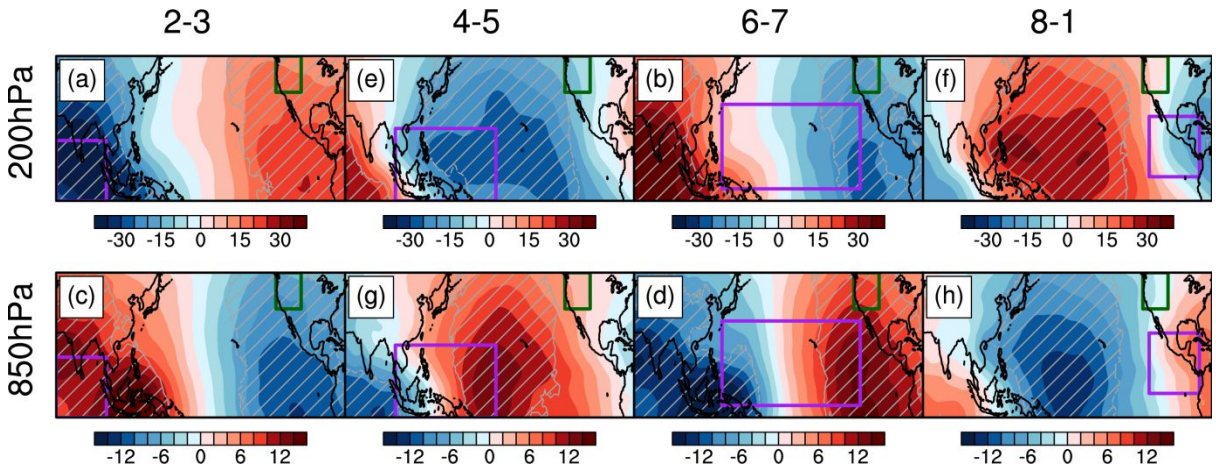

Figure S2. Same as Fig. 6 in the manuscript but gray hatching enclosed with contours displays the grid points where two thirds of sample days have the same sign (either plus or minus) OLR anomalies.

For Review Only

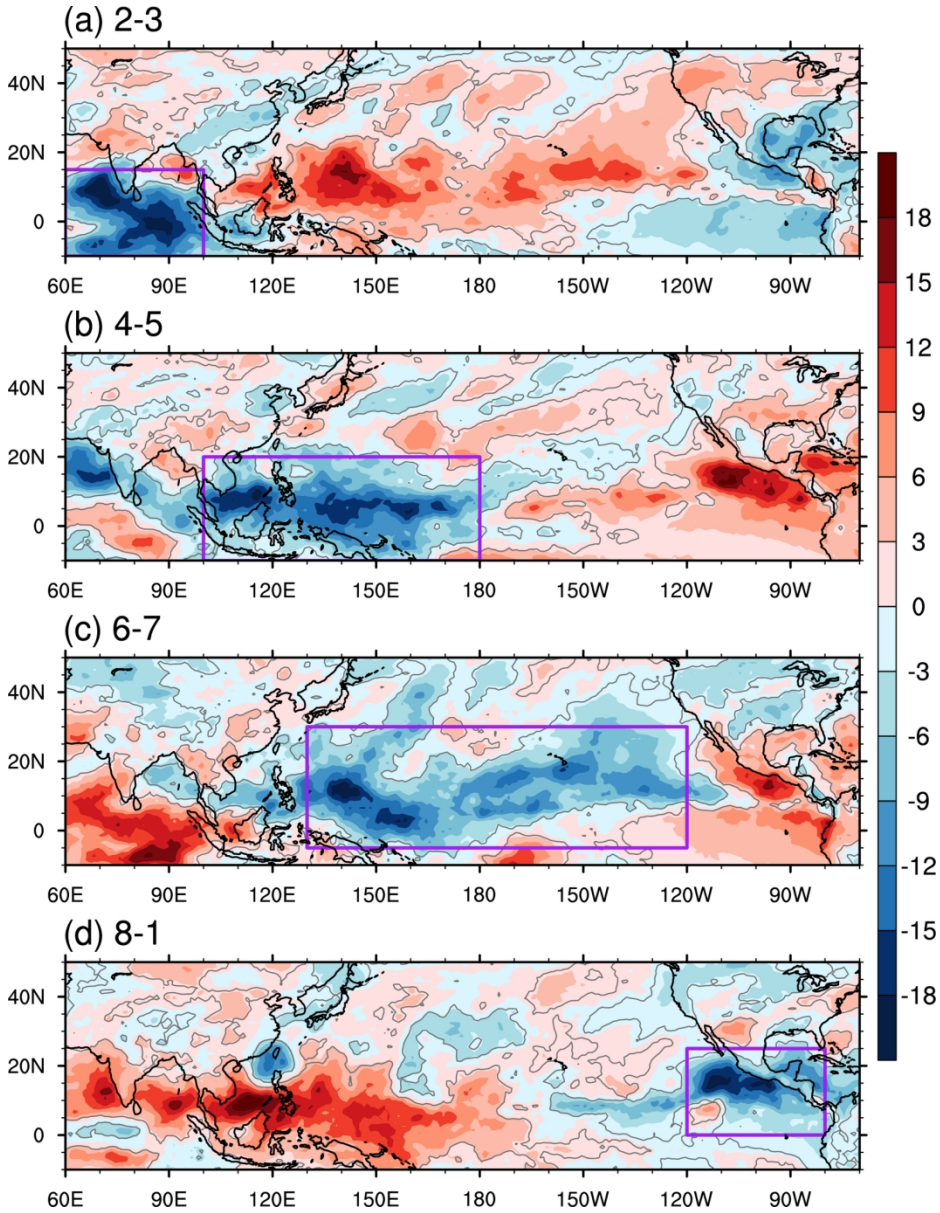

Figure 1. OLR anomaly composites from MJO events onset date for four MJO phase pairs during 1979-2010 summer seasons. An MJO event must last at least three days, have RMM≥1, and be separated ≥10 days from another event. The unit of shading is Wm-2. Areas enclosed with grey contours are significant at the 95% confidence level according to the two-tailed student's t-test. Purple boxes show areas of larger OLR magnitude for each MJO phase pair.

145x187mm (300 x 300 DPI)

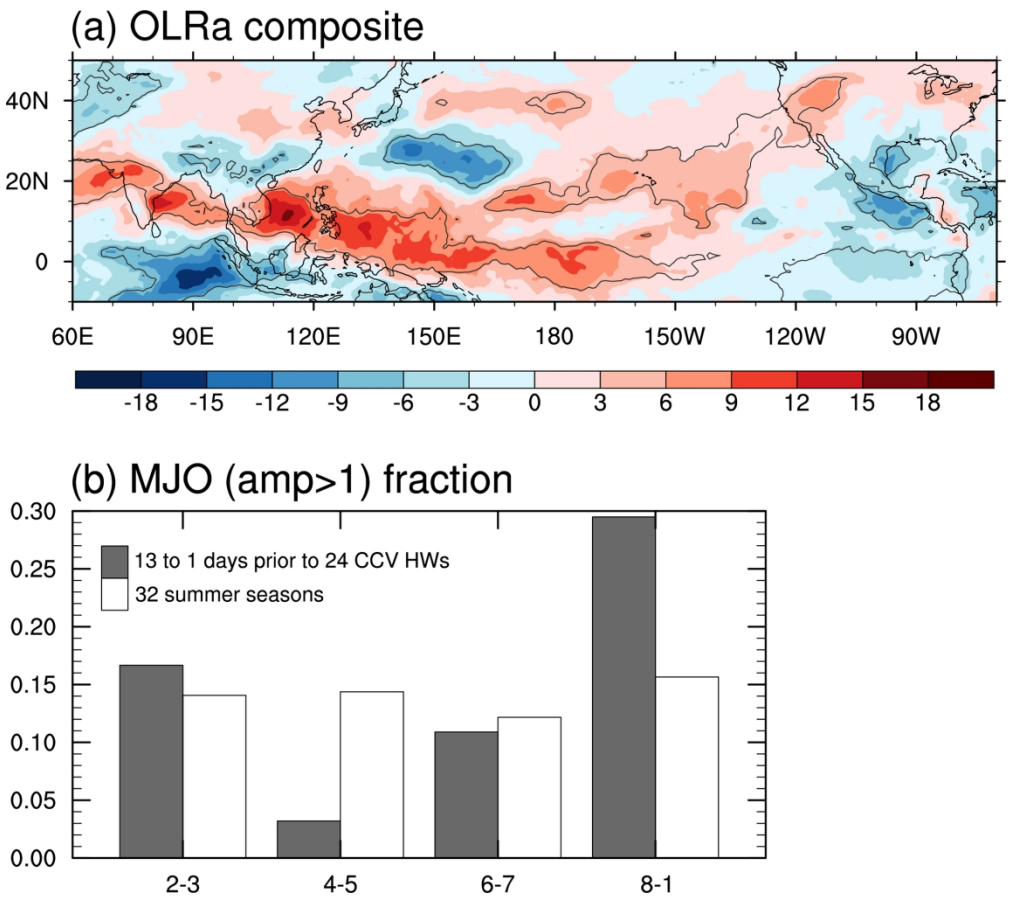

Figure 2. (a) OLR anomaly composite during the 13 days prior to 24 CCV HW events onset. The unit of shading is Wm-2. Areas enclosed with grey contours are significant at the 95% confidence level according to the two-tailed student's t-test. (b) Fraction of active MJO days with RMM amplitde ≥1 for each of four phase pairs out of (dark grey) 13 days prior to all 24 HW onset dates and among (light grey) all 32 seasons of summer days.

186x164mm (300 x 300 DPI)

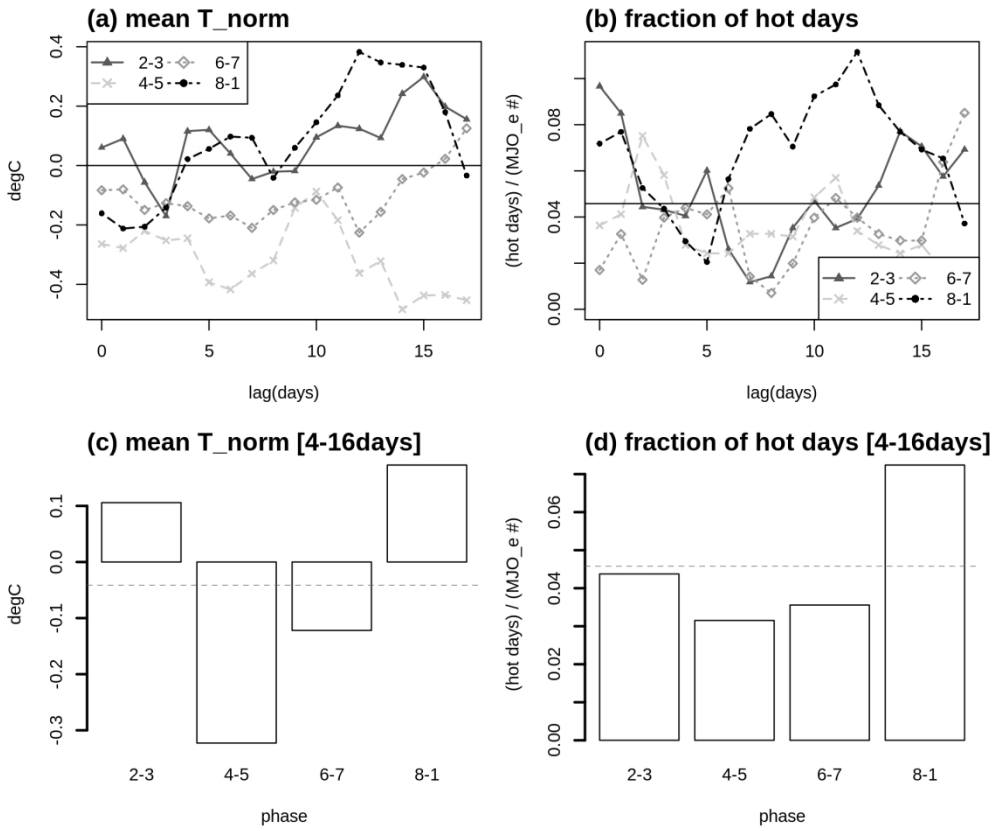

Figure 3. Temporal evolution of (a) mean normalized temperature anomalies and (b) fraction of hot days averaged over 15 CCV stations after MJO events onset during four phase pairs. Lag 1 is the day following the onset date of each individual MJO event. The average of (a) and (b) for 4-16 lag days are shown in (c) and (d). Horizontal dashed line denotes the average of four phase pairs in (c) and (d).

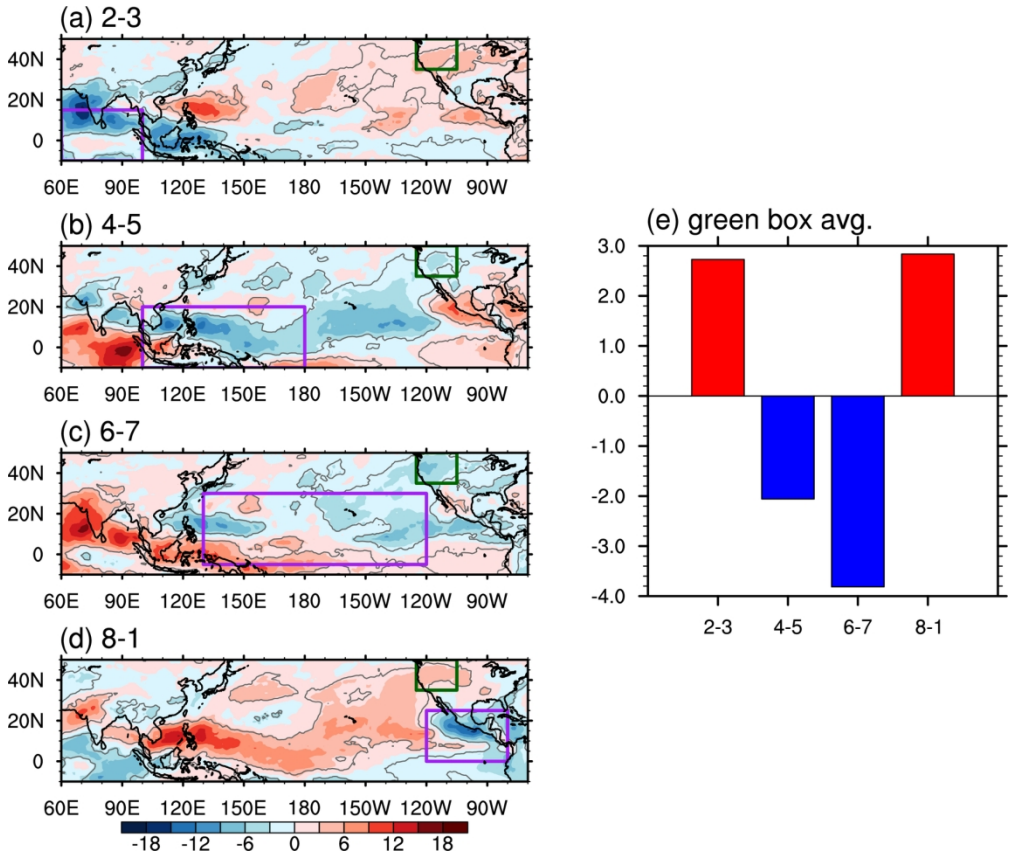

Figure 4. (a-d) OLR anomaly composites of 4-16 days after all MJO events onset dates and (e) area averaged OLR anomalies over the green boxed area for each of four phase pairs. Areas enclosed with grey contours in (a-d) are significant at the 95% confidence level according to the two-tailed student's t-test. Purple boxes show areas of larger OLR magnitude in corresponding phase pairs (shown in Figure 1). The green box shows an area of larger OLR magnitude near the CCV (125°W-105°W, 35°N-50°N).

162x136mm (300 x 300 DPI)

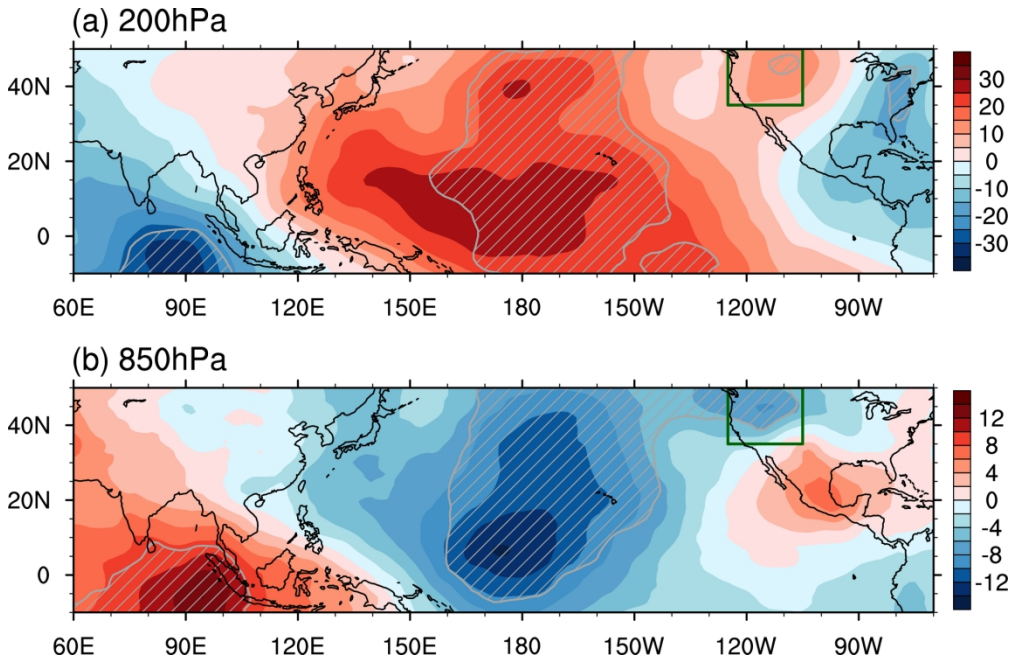

Figure 5. VP anomaly composites from all 24 CCV HW events onset for (a) 200 hPa and (b) 850 hPa. The unit of shading is 105 m2s-1. Hatched areas enclosed with contours are significant at the 95% confidence level according to the two-tailed student's t-test.

186x120mm (300 x 300 DPI)

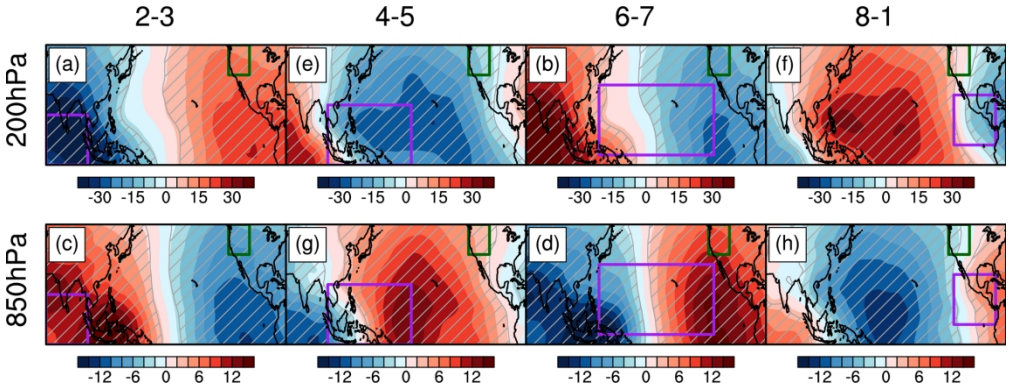

Figure 6. VP anomaly composites of 4-16 days after all MJO events onset date for four phase pairs at (a,e,b,f) 200 hPa and (c,g,d,h) 850 hPa. The unit of shading is 105 m2s-1. Hatched areas enclosed with contours are significant at the 95% confidence level according to the two-tailed student's t-test. Purple boxes show areas of larger OLR magnitude in corresponding phase pairs (as in Figure 1).

190x71mm (300 x 300 DPI)

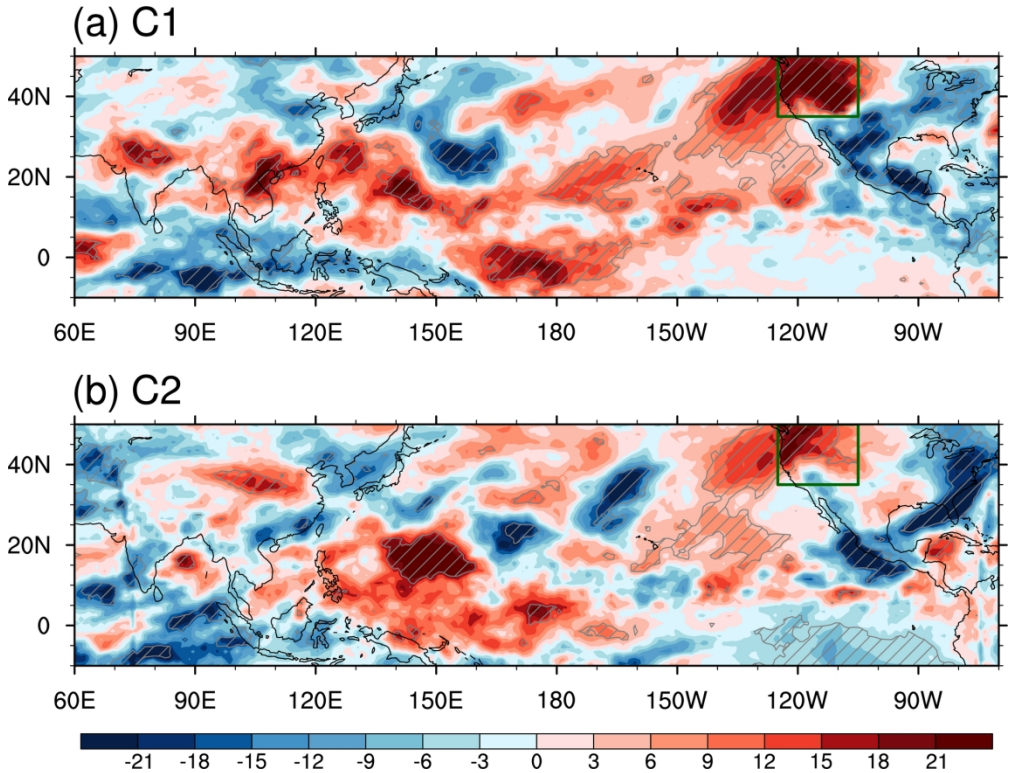

Figure 7. OLR anomaly composites during 3 days from CCV HW events onset for (a) Custer 1 and (b) Cluster 2. The unit of shading is Wm-2. Hatched areas enclosed with contours are significant at the 95% confidence level according to the two-tailed student's t-test.

186x142mm (300 x 300 DPI)

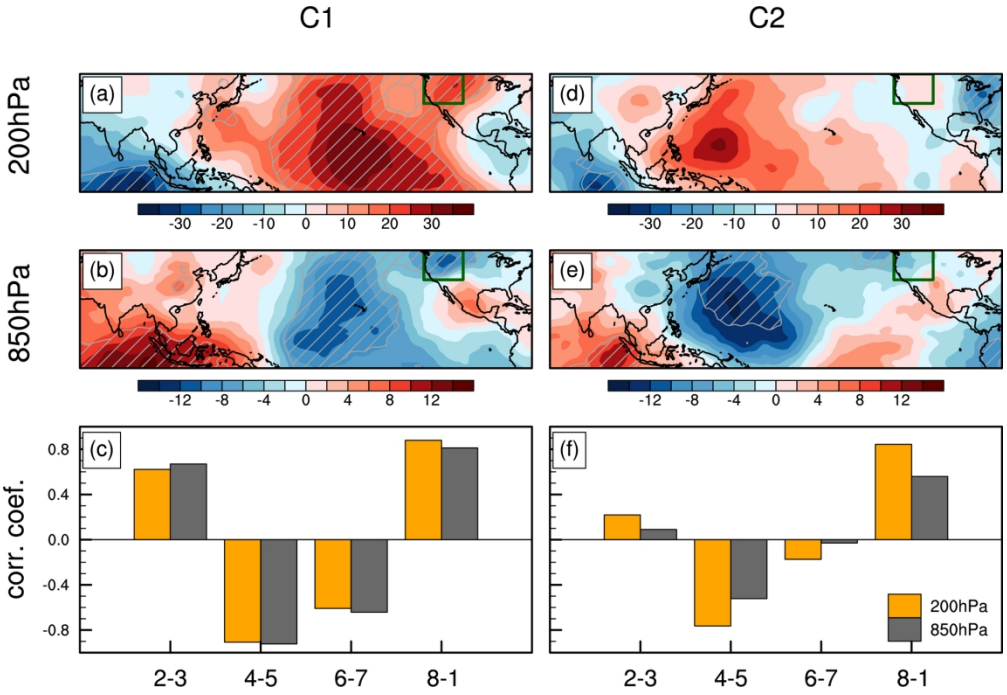

Figure 8. VP anomaly composites during 3 days from CCV HW events onset similar to Figure 5 but for each of two clusters at (a, d) 200 hPa and (b, e) 850 hPa. The unit of shading is 105 m2s-1. Hatched areas enclosed with contours are significant at the 95% confidence level according to the two-tailed student's t-test. Bars in (c,f) show pattern correlation coefficients between individual VP field of two CCV HW clusters (a,b,d,e) and the VP field during 4-16 days after MJO events for each of four phase pairs (shown in Figure 6) over the whole domain (60°E-70°W, 10°S-50°N). Orange and dark gray bars are for 200 hPa and 850 hPa, respectively.

182x124mm (300 x 300 DPI)